



CERN-EP-2022-082
 LHCb-PAPER-2022-007
 September 22, 2023

Measurement of the prompt D^0 nuclear modification factor in $p\text{Pb}$ collisions at $\sqrt{s_{\text{NN}}} = 8.16 \text{ TeV}$

LHCb collaboration[†]

Abstract

The production of prompt D^0 mesons in proton-lead collisions in both the forward and backward rapidity regions at a center-of-mass energy per nucleon pair of $\sqrt{s_{\text{NN}}} = 8.16 \text{ TeV}$ is measured by the LHCb experiment. The nuclear modification factor of prompt D^0 mesons is determined as a function of the transverse momentum p_T , and the rapidity in the nucleon-nucleon center-of-mass frame y^* . In the forward rapidity region, significantly suppressed production with respect to pp collisions is measured, which provides significant constraints on models of nuclear parton distributions and hadron production down to the very low Bjorken- x region of $\sim 10^{-5}$. In the backward rapidity region, a suppression with a significance of 2.0–3.8 standard deviations compared to nPDF expectations is found in the kinematic region of $p_T > 6 \text{ GeV}/c$ and $-3.25 < y^* < -2.5$, corresponding to $x \sim 0.01$.

Published in Phys. Rev. Lett. **131** (2023) 102301.

© 2023 CERN for the benefit of the LHCb collaboration. CC BY 4.0 licence.

[†]Authors are listed at the end of this Letter.

Charm and beauty quarks are produced in the early stage of ultra-relativistic heavy-ion collisions and are strongly affected by the presence of deconfined hot nuclear matter, known as quark-gluon plasma (QGP) [1], as well as by cold nuclear matter (CNM) effects. The latter can be studied in proton-nucleus collisions where QGP effects are not expected to be dominant. Heavy-flavor hadrons, *i.e.* hadrons containing one or more heavy quark, are affected by CNM effects at all stages of their production. At LHC energies, the most relevant effect is from the initial state, where the parton distribution functions in a nuclear environment (nPDF) [2–4] differ from those in isolated nucleons at all values of Bjorken momentum fraction x . Parton density decreases at $x \lesssim 0.1$ due to nuclear shadowing, and increases at $0.1 \lesssim x \lesssim 0.3$ as a result of antishadowing [5]. Therefore different effects are expected to be relevant at different intervals of rapidity, which is strongly correlated with x . The parton distributions at small x can also be described by the color-glass condensate effective theory (CGC) as a saturated gluonic system [6]. Moreover, multiple scattering and energy loss may occur when the incoming partons and the heavy quarks traverse the nuclear medium [7–9]. Other initial-state or even final-state effects [10, 11] may also modify the kinematic distributions of produced heavy-flavor hadrons, as suggested by their surprisingly large spatial anisotropy in momentum in high-multiplicity $p\text{Pb}$ collisions [12, 13].

The LHCb collaboration has recently measured the production cross-section of various heavy-flavor hadrons in $p\text{Pb}$ collisions at forward rapidity, including the production of prompt D^0 and Λ_c^+ hadrons at a center-of-mass energy per nucleon pair of $\sqrt{s_{\text{NN}}} = 5.02 \text{ TeV}$ [14, 15], and the production of J/ψ , B^0 , B^+ , Λ_b^0 and $\Upsilon(nS)$ states at $\sqrt{s_{\text{NN}}} = 8.16 \text{ TeV}$ [16–18]. The ALICE collaboration has measured open charm production at midrapidity at $\sqrt{s_{\text{NN}}} = 5.02 \text{ TeV}$ [19–24]. Other measurements of heavy-flavor production in $p\text{Pb}$ collisions at the LHC are also reported [25–36]. CNM effects have also been investigated with heavy-quark production at the RHIC collider in $d\text{Au}$ collisions at $\sqrt{s_{\text{NN}}} = 200 \text{ GeV}$ [37, 38]. These measurements have led to significantly reduced uncertainties of nPDFs in the small- x region [39, 40], especially with the constraints from the LHCb D^0 measurements at $\sqrt{s_{\text{NN}}} = 5.02 \text{ TeV}$ [14].

This Letter reports the measurement of the production cross-section and the nuclear modification factor $R_{p\text{Pb}}$ of prompt D^0 mesons in $p\text{Pb}$ collisions at $\sqrt{s_{\text{NN}}} = 8.16 \text{ TeV}$ performed with the LHCb detector [41]. The quantity $R_{p\text{Pb}}$ is defined as the ratio of the cross-section in $p\text{Pb}$ collisions to the corresponding cross-section in pp collisions scaled by the mass number of Pb. Prompt mesons are those directly produced in proton-lead collisions or from strong decays of excited charm hadrons, rather than from decays of beauty hadrons. This measurement uses a data sample 20 times larger than that used for the LHCb D^0 measurements at $\sqrt{s_{\text{NN}}} = 5.02 \text{ TeV}$ [14]. The results can be incorporated into global fits together with all other relevant measurements to improve nPDF parameterizations and to test other possible CNM effects.

The LHCb detector is a single-arm forward spectrometer designed for studying heavy-flavor particles, described in detail in Refs. [41, 42]. The data sample for this analysis consists of $p\text{Pb}$ collisions collected with the LHCb detector at the end of 2016, including two different configurations: forward collisions (p beam coming from upstream of the vertex detector) and backward collisions (p beam coming from downstream of the vertex detector), corresponding to an integrated luminosity of $12.2 \pm 0.3 \text{ nb}^{-1}$ ($18.6 \pm 0.5 \text{ nb}^{-1}$) for forward (backward) collisions [17, 43]. The forward (backward) configuration data cover a positive (negative) rapidity range of $1.5 < y^* < 4.0$ ($-5.0 < y^* < -2.5$), corresponding

to an x coverage of approximately $10^{-5} - 10^{-3}$ ($10^{-2} - 10^{-1}$) for the partons of the Pb nucleus, with the positive z -axis defined as the direction of the proton beam.

Simulation samples are required to model the effects of the detector acceptance and the selection requirements. The D^0 mesons are generated using PYTHIA 8 [44] with a specific LHCb configuration [46] and embedded into minimum-bias $p\text{Pb}$ events from the EPOS-LHC generator [45]. Decays of unstable particles are described by EVTGEN [47], in which final-state radiation is generated using PHOTOS [48]. The interaction of the generated particles with the detector, and its response, are implemented using the GEANT4 toolkit [49] as described in Ref. [50].

The double differential cross-section for prompt D^0 production is measured as a function of y^* , the rapidity in the nucleon-nucleon center-of-mass frame, and p_{T} , the transverse momentum with respect to the beam direction. The quantity y^* is related to the rapidity in the laboratory frame y_{lab} by $y^* = y_{\text{lab}} - 0.465$ for $p\text{Pb}$ collisions. The differential cross-section in a given (p_{T}, y^*) interval is defined as

$$\frac{d^2\sigma}{dp_{\text{T}}dy^*} \equiv \frac{N(D^0 \rightarrow K^\mp\pi^\pm) + N(\overline{D}^0 \rightarrow K^\pm\pi^\mp)}{\mathcal{L} \times \varepsilon_{\text{tot}} \times \mathcal{B}(D^0 \rightarrow K^\mp\pi^\pm) \times \Delta p_{\text{T}} \times \Delta y^*}, \quad (1)$$

where $N(D^0 \rightarrow K^\mp\pi^\pm)$ and $N(\overline{D}^0 \rightarrow K^\pm\pi^\mp)$ are the D^0 and \overline{D}^0 signal yields, \mathcal{L} is the integrated luminosity, ε_{tot} is the total efficiency, $\mathcal{B}(D^0 \rightarrow K^\mp\pi^\pm) = (3.96 \pm 0.03)\%$ is the sum of branching fractions for the decays $D^0 \rightarrow K^-\pi^+$ and $D^0 \rightarrow K^+\pi^-$ [51], and Δp_{T} and Δy^* are the p_{T} and y^* interval widths. The D^0 mesons are reconstructed through the $D^0 \rightarrow K^-\pi^+$ and the doubly Cabibbo-suppressed $D^0 \rightarrow K^+\pi^-$ decay channels and their charge conjugates ¹. The measurement is performed within a p_{T} range of $0 < p_{\text{T}} < 30 \text{ GeV}/c$, and the rapidity range defined above. Throughout the analysis, the measurements are for the combined sample of D^0 and \overline{D}^0 mesons. The signal yields and the total efficiency are determined in each kinematic interval.

The D^0 candidates are built from K^\mp and π^\pm candidate tracks. The selection criteria are similar to those used in D^0 production measurements in $p\text{Pb}$ collisions at $\sqrt{s_{\text{NN}}} = 5.02 \text{ TeV}$ [14]. The reconstructed K^\mp and π^\pm tracks are required to have transverse momentum greater than $0.4 \text{ GeV}/c$. Both tracks are also required to be of good quality, come from a common vertex, and pass particle identification (PID) requirements.

The inclusive D^0 signal yield is the sum of the prompt D^0 mesons and those produced in the decays of b hadrons, denoted “from- b ”. This inclusive yield is determined using an extended unbinned maximum-likelihood fit to the distribution of the $K\pi$ invariant mass, $M(K\pi)$. The $M(K\pi)$ distribution of the signal is described by a sum of a Crystal Ball function [52] and a Gaussian function sharing a common mean value, while the background shape is described by a linear function, following the measurement of Ref. [14]. The prompt signal yield is determined by fitting the distribution of $\log_{10}(\chi_{\text{IP}}^2)$ of the D^0 candidates, where χ_{IP}^2 is defined as the difference in the vertex-fit χ^2 of a given primary vertex reconstructed with and without the D^0 candidate under consideration. The background component in the $\log_{10}(\chi_{\text{IP}}^2)$ distribution is subtracted using the *sPlot* technique [53] with $M(K\pi)$ as the discriminating variable. The shapes of the $\log_{10}(\chi_{\text{IP}}^2)$ distribution corresponding to the prompt and *from-b* components are described independently by Bukin functions [54], which are asymmetric functions with tails described by Gaussian

¹The branching fraction of $D^0 \rightarrow K^+\pi^-$ channel is two orders of magnitude smaller than that of $D^0 \rightarrow K^-\pi^+$.

functions. The parameters of the functions describing the prompt and *from-b* components are fixed to those from simulation. The invariant-mass and $\log_{10}(\chi^2_{\text{IP}})$ distributions of the forward and backward samples are given in the Supplemental Material [55].

The total efficiency ε_{tot} is the product of the geometrical acceptance of the detector, the selection and reconstruction efficiency, the PID efficiency and the trigger efficiency, with each component determined separately. The geometrical acceptance, and the selection, reconstruction and trigger efficiencies are evaluated with the $p\text{Pb}$ simulation samples. The simulation sample is weighted in order to match the occupancy of the tracking system observed in the data. The track reconstruction efficiency is calibrated with minimum-bias $J/\psi \rightarrow \mu^+ \mu^-$ and $K_S^0 \rightarrow \pi^+ \pi^-$ samples, using the tag-and-probe approach employed in Ref. [56]. The trigger efficiency obtained from the simulation is validated by measuring it from control data samples recorded with minimum trigger requirements. The PID efficiency is estimated with a tag-and-probe method [57, 58], using the D^* -tagged decay chain $D^{*+} \rightarrow D^0 \pi^+$ with $D^0 \rightarrow K^- \pi^+$ decays.

Several sources of systematic uncertainty are considered and described in detail in the Supplemental Material [55], where results and numerical values for the double-differential cross-section are also given. The total prompt D^0 production cross-section, obtained by integrating the double-differential measurements, is $297.6 \pm 0.6 \pm 14.0$ mb in the kinematic range of $0 < p_T < 30$ GeV/ c and $1.5 < y^* < 4.0$ for the forward rapidity region, and $315.2 \pm 0.2 \pm 17.8$ mb in the kinematic range of $0 < p_T < 30$ GeV/ c and $-5.0 < y^* < -2.5$ in the backward rapidity region. The first uncertainties are statistical and the second systematic.

The nuclear modification factor $R_{p\text{Pb}}$ is defined as

$$R_{p\text{Pb}}(p_T, y^*) \equiv \frac{1}{A} \frac{d^2\sigma_{p\text{Pb}}(p_T, y^*)/(dp_T dy^*)}{d^2\sigma_{pp}(p_T, y^*)/(dp_T dy^*)}, \quad (2)$$

where $A = 208$ is the mass number of the lead nucleus and σ_{pp} is the prompt D^0 production cross-section in pp collisions at $\sqrt{s} = 8.16$ TeV. An interpolation between LHCb measurements at $\sqrt{s} = 5.02$ TeV and $\sqrt{s} = 13$ TeV [59, 60] is performed to obtain $d^2\sigma_{pp}(p_T, y^*)/(dp_T dy^*)$, using a power-law function $\sigma(\sqrt{s}) = p_0(\sqrt{s})^{p_1}$. A linear function is also considered. The interpolation uncertainty comprises the difference between the two interpolation models, and the propagated total uncertainties from the pp measurements, and typically amounts to 3% (5%) at forward (backward) rapidity. The interpolation is performed within the common measured kinematic range of $p_T < 10$ GeV/ c and $2.0 < y < 4.5$ for 5.02 and 13 TeV pp results, hence $R_{p\text{Pb}}$ is measured in that range.

The nuclear modification factor of the D^0 meson as a function of p_T is displayed in Fig. 1, where 8 panels report the results in different y^* subintervals of $\Delta y^* = 0.5$ and the two left panels are in the common range between the forward and backward rapidity coverage, $2.5 < |y^*| < 4$. Figures showing $R_{p\text{Pb}}$ and the forward-backward production ratio R_{FB} as functions of y^* and p_T in $\Delta y^* = 0.25$ intervals, as well as the numerical values are given in the Supplemental Material [55]. A significant suppression of the cross-section in $p\text{Pb}$ collisions, with respect to that in pp collisions scaled by the lead mass number, is observed at forward rapidity as well as at backward rapidity up to $y^* \sim -3.5$.

The $R_{p\text{Pb}}$ results are compared with several theoretical calculations. The HELAC-Onia approach [62, 63] is based on a data-driven modeling of the scattering at partonic level folded with the free proton PDFs [66]. The calculations are first tuned by fitting the cross-sections measured in pp collisions at the LHC. Then, the modified PDFs of

nucleons in the Pb nucleus are introduced in the model to calculate the cross-sections in $p\text{Pb}$ collisions and to estimate the effect of nPDFs, neglecting other cold and hot nuclear matter effects. Reweighted EPPS16 [64] and nCTEQ15 [65] nPDF sets, where LHC heavy flavor data [14, 19–21] are incorporated by performing a Bayesian-reweighting analysis [61], are used in the calculations, resulting in considerably reduced uncertainties than calculations using the default nPDFs. The uncertainties are dominated by nPDF parameterizations and correspond to a 68% confidence interval. At forward rapidity, the calculations are in general agreement with the data, except for $p_{\text{T}} < 1 \text{ GeV}/c$ where the predictions are about 2 standard deviations larger than the data. This discrepancy suggests stronger shadowing or additional energy loss at low x . At backward rapidity, for $p_{\text{T}} > 6 \text{ GeV}/c$ and $-3.5 < y^* < -2.5$ the data are lower than the calculations by $2.0 - 3.8$ standard deviations, indicating a weaker antishadowing effect or possible final-state effects.

The nuclear modification factor is also compared with two calculations based on the CGC effective field theory, CGC1 and CGC2. Since gluon saturation is expected to occur at small x and Q^2 , the calculations are applicable for $p_{\text{T}} < 5 \text{ GeV}/c$ at forward rapidity where saturation effects are relevant. For CGC1 [67, 68] the D -meson production is calculated with the color dipole formalism, and the optical Glauber model is used to relate the initial condition of a nucleus to that of the proton. For CGC2 [69] the color dipole approach is combined with a heavy-quark fragmentation function to calculate the cross-sections. The CGC1 predictions have much smaller uncertainties than the CGC2 ones, because the CGC1 uncertainties include only variations of the c quark mass and of the factorization scale, which largely cancel out in the $R_{p\text{Pb}}$ ratio versus p_{T} . CGC1 is consistent with the upper bound of CGC2 and is slightly higher than the data. CGC2 shows a stronger suppression than HELAC-Onia calculations and gives a better description of the data, especially for $p_{\text{T}} < 3 \text{ GeV}/c$.

A fourth calculation estimates D^0 suppression caused by medium-induced fully coherent energy loss (FCEL) [9], a CNM effect where the interference between initial- and final-state gluon radiation results in an energy loss proportional to the incoming parton energy. The FCEL prediction shown in Fig. 1 does not consider the modification of nPDFs. The effect is significant for low p_{T} , suggesting the suppression observed for $p_{\text{T}} < 1 \text{ GeV}/c$ may be caused by combined effects from nPDFs and FCEL. For $p_{\text{T}} > 6 \text{ GeV}/c$ the suppression due to FCEL is negligible, thus the discrepancy between the data and HELAC-Onia calculations with nPDFs at backward rapidity cannot be attributed to FCEL effects.

The results are also compared with the LHCb D^0 measurement at $\sqrt{s_{\text{NN}}} = 5.02 \text{ TeV}$ [14]. At forward rapidity the $R_{p\text{Pb}}$ values at the two energies are compatible, while at backward rapidity the 8.16 TeV data are significantly lower. The difference could be related to the different Bjorken- x coverage at the two collision energies, while effects related to the Pb-going hemisphere other than nPDFs and FCEL, such as final-state energy loss in a high-particle-density environment, may also show a $\sqrt{s_{\text{NN}}}$ dependence as more charged hadrons are produced in 8.16 TeV collisions. On the other hand, the model calculations offer limited insights into collision energy dependence. HELAC-Onia predictions based on nPDFs are compatible between the two $\sqrt{s_{\text{NN}}}$ values due to the large uncertainty of the nPDFs used in the 5.02 TeV calculation. The CGC models show similar values at 5.02 and 8.16 TeV at forward rapidity while they are not applicable at backward. Effects due to FCEL are generally small at backward rapidity.

It is essential to study the impact of Bjorken- x coverage in order to interpret the energy dependence observed in the data. However, x and the momentum transfer Q^2 [5]

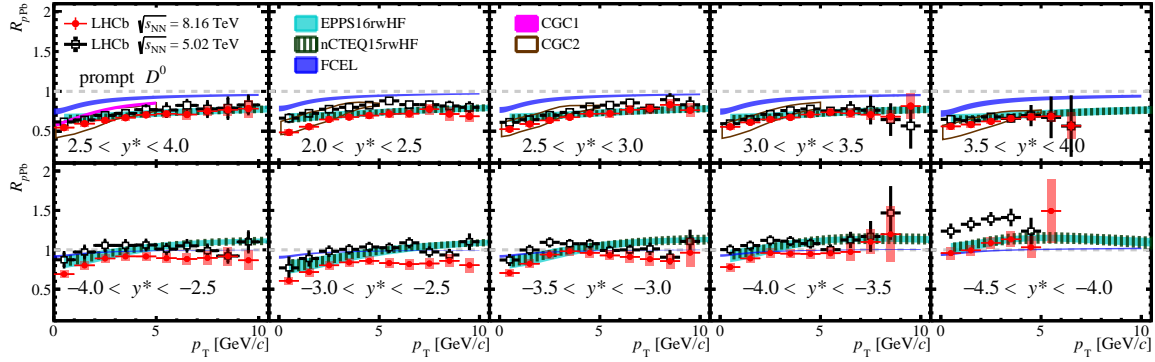


Figure 1: Nuclear modification factor as a function of p_T in different y^* intervals for prompt D^0 mesons in the (top) forward and (bottom) backward regions. The error bars show the statistical uncertainties and the boxes show the systematic uncertainties. The LHCb results at $\sqrt{s_{NN}} = 5.02$ TeV [14] and theoretical calculations at $\sqrt{s_{NN}} = 8.16$ TeV from Refs. [9, 64, 65, 68, 69] are also shown. For LHCb results at $\sqrt{s_{NN}} = 5.02$ TeV, the error bars show the quadric sum of statistical and systematic uncertainties.

are partonic quantities that cannot be directly measured in hadronic collisions. Instead, experimental proxies x_{exp} and Q_{exp}^2 , defined as

$$x_{\text{exp}} \equiv 2 \frac{\sqrt{p_T^2(D^0) + M^2(D^0)}}{\sqrt{s_{NN}}} e^{-y^*} \quad \text{and} \quad Q_{\text{exp}}^2 \equiv p_T^2(D^0) + M^2(D^0), \quad (3)$$

are introduced to approximate the variation of $R_{p\text{Pb}}$ with x and Q^2 , where $M(D^0)$ and $p_T(D^0)$ denote the mass and p_T of D^0 mesons, respectively.

Figure 2 shows $R_{p\text{Pb}}$ as a function of x_{exp} in five Q_{exp}^2 intervals, for D^0 mesons measured in this work at 8.16 TeV, and at 5.02 TeV from Ref. [14]. The x_{exp} coverage of the 8.16 TeV data extends lower than that of the 5.02 TeV measurements due to the higher $\sqrt{s_{NN}}$ value, reaching down to $x_{\text{exp}} \sim 10^{-5}$ in the interval $3.48 < Q_{\text{exp}}^2 < 7.48$ GeV 2 , which corresponds to $p_T < 2$ GeV/ c . The 8.16 TeV data are also more precise. Data from the two energies are in good agreement with each other at common x_{exp} values. The measurements form a consistent trend from the small x_{exp} region corresponding to forward rapidity to the large x_{exp} region corresponding to backward rapidity, for all Q_{exp}^2 intervals. The $D^0 R_{p\text{Pb}}$ ratio at 5.02 TeV at midrapidity [22] measured by the ALICE collaboration is also added to Fig. 2, and is compatible with the trend within uncertainties. The trend suggests that the $\sqrt{s_{NN}}$ dependence observed at backward rapidity in Fig. 1 arises from different x coverage in a kinematic region where $R_{p\text{Pb}}$ depends strongly on x .

The HELAC-Onia predictions are also transformed according to Eq. 3 and shown in Fig. 2. In the small x_{exp} region, the calculations are in general agreement with the data, except for the interval $3.48 < Q_{\text{exp}}^2 < 7.48$ GeV 2 ($p_T < 2$ GeV/ c) and $10^{-5} < x_{\text{exp}} < 10^{-4}$, where the nPDF expectations are slightly larger than the data and show greater uncertainty. The data hint at a stronger shadowing effect, or other possible effects such as FCEL, that suppresses low- p_T D^0 production at forward rapidity. Moreover, estimations from Ref. [70] suggest gluon saturation may occur in this region. At backward rapidity, the $R_{p\text{Pb}}$ values from the model are larger than those in the data for $Q_{\text{exp}}^2 > 19.48$ GeV 2 ($p_T > 4$ GeV/ c) and $10^{-2} < x_{\text{exp}} < 10^{-1}$, indicating smaller antishadowing effects in the data if nuclear

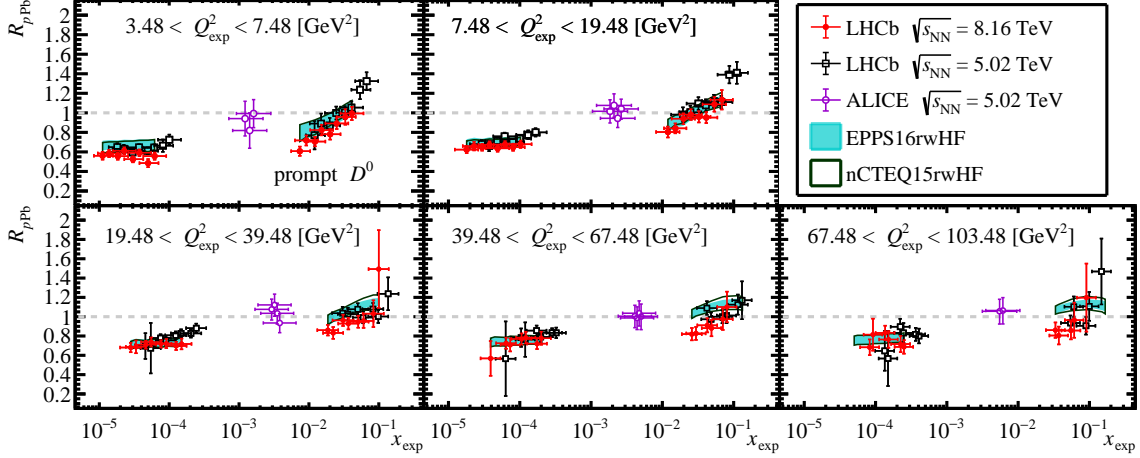


Figure 2: Nuclear modification factor as a function of x_{exp} in different Q_{exp}^2 intervals for prompt D^0 mesons for LHCb results at $\sqrt{s_{\text{NN}}} = 8.16$ TeV and $\sqrt{s_{\text{NN}}} = 5.02$ [14] and the ALICE result at $\sqrt{s_{\text{NN}}} = 5.02$ TeV [22]. Theoretical calculations at $\sqrt{s_{\text{NN}}} = 8.16$ TeV from Refs. [64, 65] are also shown. The horizontal error bars account for the maximum and minimum x_{exp} values for a given (p_{T}, y^*) interval and the vertical error bars show the quadric sum of statistical and systematic uncertainties.

effects other than nPDFs are negligible. Alternatively it suggests additional suppression mechanisms, such as final-state energy loss, may occur at backward rapidity.

In summary, the prompt D^0 production cross-section is measured at the LHCb experiment in proton-lead collisions at $\sqrt{s_{\text{NN}}} = 8.16$ TeV, at both forward and backward rapidities. The nuclear modification factors are measured with high accuracy and show strong cold nuclear matter effects. A stronger suppression than the predictions of nPDF calculations is observed for the lowest transverse momentum region of $p_{\text{T}} < 1$ GeV/c at forward rapidity, hinting at a stronger shadowing than predicted at Bjorken- $x \sim 10^{-5}$, or additional effects at play. For the backward rapidity range of $-3.5 < y^* < -2.5$, the $R_{p\text{Pb}}$ values are lower than nPDF calculations at $p_{\text{T}} > 6$ GeV/c with a significance of $2.0 - 3.8$ standard deviations, indicating a weaker antishadowing effect than the model or additional final-state effects at backward rapidity. This Letter presents the most precise measurement of the prompt D^0 production in $p\text{Pb}$ collisions to date, providing unique constraints to improve nPDF parameterization down to $x \sim 10^{-5}$.

Supplemental Material

Fit to $M(K\pi)$ and $\log_{10}(\chi^2_{\text{IP}})$ distributions

The fit results for the $M(K\pi)$ and $\log_{10}(\chi^2_{\text{IP}})$ distributions in the kinematic ranges of $2.5 < p_T < 3.0 \text{ GeV}/c$ and $3.25 < y^* < 3.50$ ($-4.50 < y^* < -4.25$) are shown in Fig. 3 (Fig. 4). The $M(K\pi)$ distribution of the signal is described by a sum of a Crystal Ball function [52] and a Gaussian function sharing a common mean value. The background shape is described by a linear function. The shapes of the $\log_{10}(\chi^2_{\text{IP}})$ distribution corresponding to the prompt and *from-b* components are described independently by Bukin functions [54].

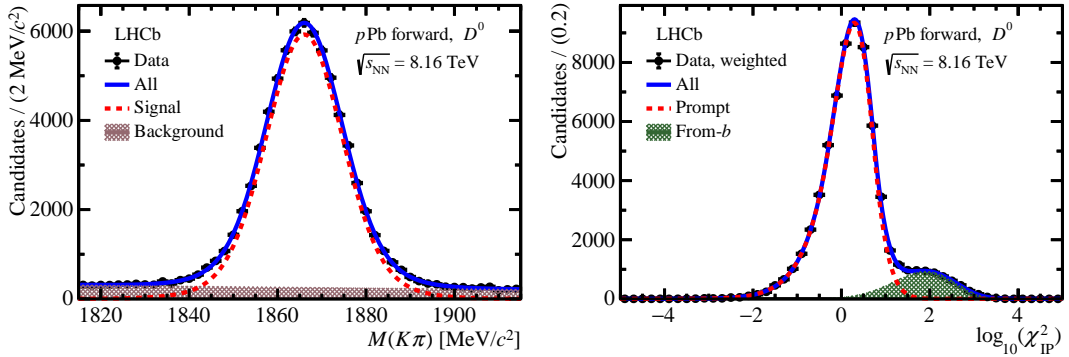


Figure 3: Distributions and fit results of (left) $M(K\pi)$ and (right) $\log_{10}(\chi^2_{\text{IP}})$ for inclusive D^0 mesons in the forward data sample in the kinematic range of $2.5 < p_T < 3.0 \text{ GeV}/c$ and $3.25 < y^* < 3.50$. For the $\log_{10}(\chi^2_{\text{IP}})$ fit, the data are weighted using the *sPlot* method to subtract the background component.

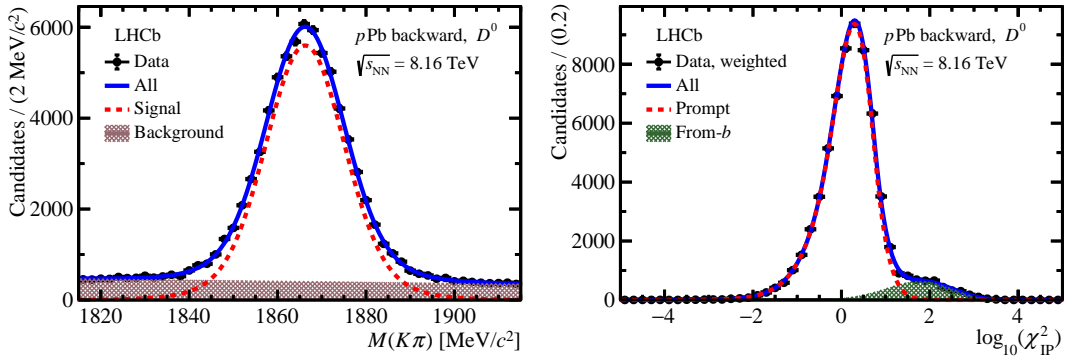


Figure 4: Distributions and fit results of (left) $M(K\pi)$ and (right) $\log_{10}(\chi^2_{\text{IP}})$ for inclusive D^0 mesons in the backward data sample in the kinematic range of $2.5 < p_T < 3.0 \text{ GeV}/c$ and $-4.50 < y^* < -4.25$. For the $\log_{10}(\chi^2_{\text{IP}})$ fit, the data are weighted using the *sPlot* method to subtract the background component.

Systematic uncertainties

Several sources of systematic uncertainty are considered and are evaluated separately for the forward and backward samples, unless stated otherwise. The systematic uncertainty due to the invariant mass $M(K\pi)$ modelling is studied using alternative models. The sum of two Crystal Ball functions [52] is used to describe the signals, and an exponential function used to describe the background. For the fit to the $\log_{10}(\chi^2_{\text{IP}})$ distribution, the parameters describing the tail of the Bukin functions [54] and the parameter describing the asymmetry of the *from-b* component, which are fixed to values derived from the simulation in the default result, are varied by one standard deviation. The effect due to the *from-b* component modelling is studied by substituting the nominal Bukin function with a Gaussian function. Finally, the background subtraction with the *sPlot* technique [53] is checked by performing the fit with the method described in Ref. [14], where the background is constructed with candidates in the side band. In these tests, the largest difference from the default value is considered as the systematic uncertainty. The uncertainties of the tracking and PID calibration are dominated by those arising from the statistically limited calibration sample size. The uncertainty arising from matching the simulated detector occupancy distribution to the data is estimated by weighting with different variables. For the trigger efficiency, the difference between the efficiencies derived from the simulation and from collision data [?] is considered as the uncertainty. The uncertainties arising from the luminosity, the $\mathcal{B}(D^0 \rightarrow K^\mp \pi^\pm)$ branching fractions, the statistically limited simulation sample size and the uncertainty from the pp interpolation are also included. The ranges of systematic uncertainties for the forward and backward rapidity regions are listed in Table 1.

Table 1: Systematic uncertainties considered in this measurement, in %. The range indicates the minimum and the maximum value among the two-dimensional p_T and y^* intervals. The systematic uncertainties due to simulation sample size, mass fit and $\log_{10}(\chi^2_{\text{IP}})$ fit are uncorrelated across the intervals. The other sources of systematic uncertainties are fully correlated between different intervals.

Uncertainty source	Forward [%]	Backward [%]
Tracking calibration	3.0 – 4.7	3.1 – 10.7
PID	0.2 – 6.9	0.2 – 26.5
Trigger efficiency	0.0 – 16.5	0.0 – 4.7
Multiplicity correction	0 – 9	0 – 16
Luminosity	2.6	2.5
Branching fraction	0.8	0.8
Mass fit	0.0 – 19.3	0.1 – 6.1
$\log_{10}(\chi^2_{\text{IP}})$ fit	0.3 – 19.5	0.4 – 7.0
Simulation sample size	1 – 40	1 – 26
pp interpolation	3.4 – 17.5	3.4 – 28.8

Double differential cross-section

The double differential cross-sections for prompt D^0 mesons in both forward and backward rapidity regions are shown in Fig. 5.

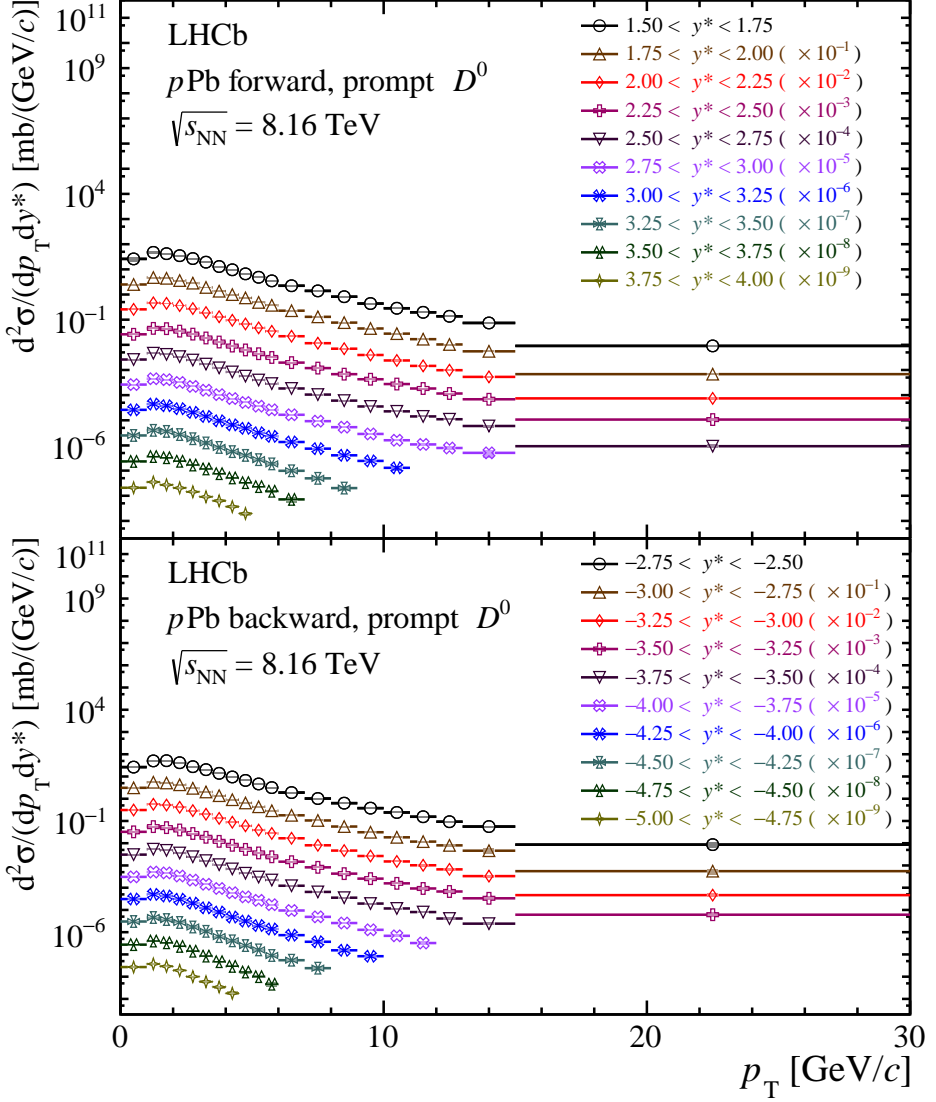


Figure 5: Double-differential cross-sections of prompt D^0 mesons in $p\text{Pb}$ collisions in the (top) forward and (bottom) backward rapidity regions. To display the differential cross-section values in different rapidity intervals, multiplicative factors of 10^{-n} are used with n increasing with rapidity value. The uncertainties are smaller than the symbol size.

Nuclear modification factor in different y^* with $\Delta y^* = 0.25$ intervals

The nuclear modification factor for the forward rapidity regions of $2.0 < y^* < 4.0$ are shown in Fig. 6 while the backward regions of $-4.5 < y^* < -2.5$ are shown in Fig. 7. The HELAC-Onia calculation [62,63] incorporating reweighted EPPS16 [64] and nCTEQ15 [65] nPDF sets, as well as the fully coherent energy loss model [9] without considering the modification of nPDFs, are included. Two color glass condensate predictions [68,69] are also shown at forward rapidity.

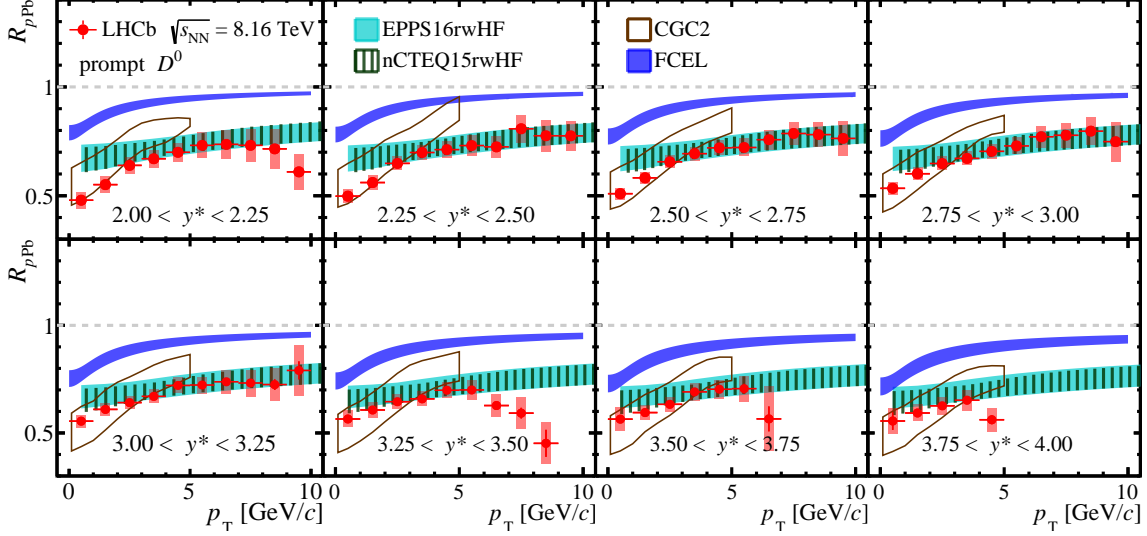


Figure 6: Nuclear modification factor as a function of p_T in different y^* intervals for prompt D^0 mesons in the forward regions for $2.0 < y^* < 4.0$. The error bars show the statistical uncertainties and the boxes show the systematic uncertainties. The theoretical calculations from Refs. [9, 64, 65, 69] are also shown.

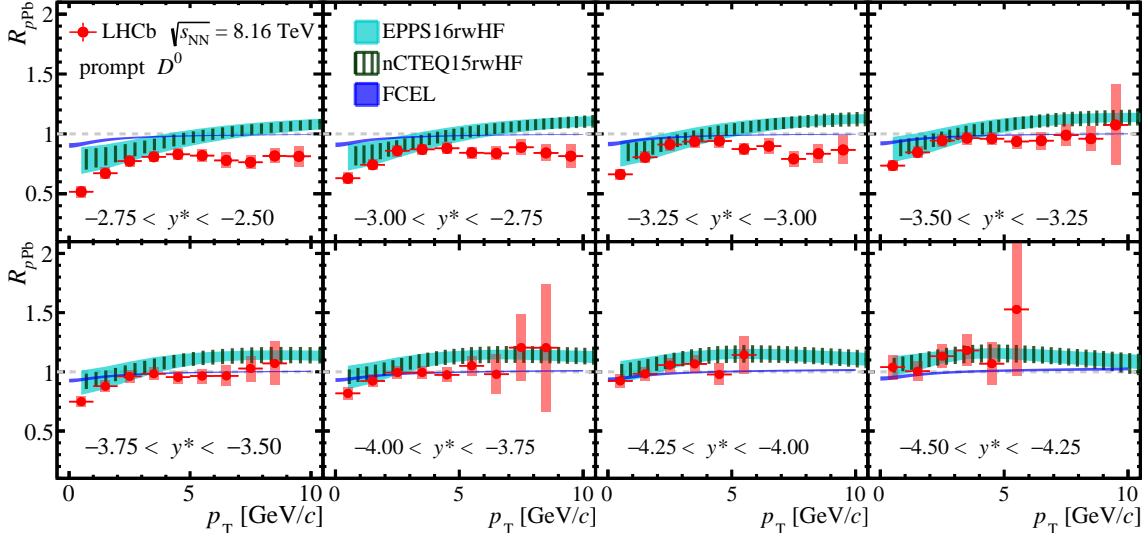


Figure 7: Nuclear modification factor as a function of p_T in different y^* intervals for prompt D^0 mesons in the backward regions for $-4.5 < y^* < -2.5$. The error bars show the statistical uncertainties and the boxes show the systematic uncertainties. The theoretical calculations from Refs. [9, 64, 65] are also shown.

Nuclear modification factor as a function of y^* intervals in full- p_T and high- p_T regions

The nuclear modification factor as a function of y^* in full- p_T ($0 < p_T < 10 \text{ GeV}/c$) and high- p_T regions ($6 < p_T < 10 \text{ GeV}/c$) are shown in Fig. 8.

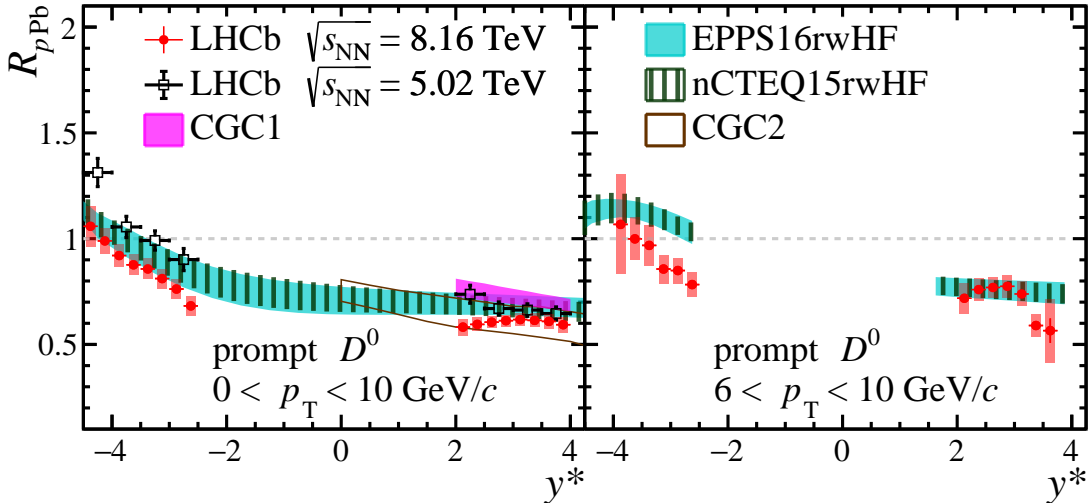


Figure 8: Nuclear modification factor for prompt D^0 mesons as a function of y^* in (left) the full- p_T range and (right) the high- p_T range. The error bars show the statistical uncertainties and the boxes show the systematic uncertainties. The LHCb results at $\sqrt{s_{\text{NN}}} = 5.02 \text{ TeV}$ [14] and theoretical calculations at $\sqrt{s_{\text{NN}}} = 8.16 \text{ TeV}$ from Refs. [64, 65, 68, 69] are also shown. For the LHCb results at $\sqrt{s_{\text{NN}}} = 5.02 \text{ TeV}$, the error bars show the quadratic sum of statistical and systematic uncertainties. On the left, the p_T range is $0 < p_T < 15 \text{ GeV}/c$ for the calculations with nPDFs of EPPS16 and nCTEQ15.

Forward-backward production ratio R_{FB}

The forward-backward production ratio is defined as

$$R_{\text{FB}}(p_T, y^*) \equiv \frac{d^2\sigma(p_T, |y^*|; y^* > 0)/(dp_T dy^*)}{d^2\sigma(p_T, |y^*|; y^* < 0)/(dp_T dy^*)}, \quad (4)$$

which is calculated in the common $|y^*|$ interval of the forward-backward acceptance, $2.5 < |y^*| < 4$. The measurements of R_{FB} are shown as a function of p_T in Fig. 9, along with the LHCb $\sqrt{s_{\text{NN}}} = 5.02 \text{ TeV}$ results [14] and the nPDF calculations. The numerical values for R_{FB} are given in Table 6. Measurements of R_{FB} vs. p_T $|y^*|$ intervals with $\Delta|y^*| = 0.25$ are shown in Fig. 10. Good agreement with nPDF calculations is found at low p_T . However, the data show a clear rising trend with increasing p_T , reaching unity at the highest p_T values, in contrast to the nPDF calculations, which predict $R_{\text{FB}} \sim 0.7$ almost independent of p_T . This difference originates from the suppression of high- p_T D^0 mesons at backward rapidity.

Tables of numerical values for the double-differential cross-section, nuclear modification factor and forward-backward ratio

The numerical values for the double-differential cross-section $d^2\sigma/(dp_T dy^*)$ are listed in Tables 2 and 3 for the forward and backward rapidity regions. The numerical values for the nuclear modification factor R_{pPb} are listed in Tables 4 and 5 for the forward and backward rapidity regions. The numerical values for the forward-backward ratio R_{FB} as a function of p_T integrated in the rapidity region of $2.5 < |y^*| < 4.0$ are listed in Table 6.

Table 2: Double-differential cross-sections for prompt D^0 mesons in intervals of p_T and y^* in forward rapidity regions. The first uncertainty is statistical, the second is the component of the systematic uncertainty that is uncorrelated across intervals and the third is the correlated component.

p_T [GeV/c]\ y^*	(1.50, 1.75)	(1.75, 2.00)	(2.00, 2.25)	(2.25, 2.50)	(2.50, 2.75)
(0.0,1.0)	26.049 \pm 1.734 \pm 1.961 \pm 4.494	25.059 \pm 0.128 \pm 0.594 \pm 1.304	25.716 \pm 0.090 \pm 0.327 \pm 1.205	26.194 \pm 0.079 \pm 0.455 \pm 1.208	26.046 \pm 0.075 \pm 0.607 \pm 1.162
(1.0,1.5)	47.452 \pm 0.229 \pm 2.317 \pm 4.304	47.375 \pm 0.222 \pm 0.870 \pm 2.639	46.707 \pm 0.160 \pm 0.630 \pm 2.243	45.091 \pm 0.137 \pm 1.369 \pm 2.000	46.465 \pm 0.138 \pm 0.780 \pm 1.999
(1.5,2.0)	42.066 \pm 0.153 \pm 1.760 \pm 2.658	41.164 \pm 0.188 \pm 0.962 \pm 2.054	44.574 \pm 0.103 \pm 0.564 \pm 1.952	43.939 \pm 0.129 \pm 0.876 \pm 2.220	41.657 \pm 0.120 \pm 0.852 \pm 1.793
(2.0,2.5)	34.993 \pm 0.350 \pm 1.535 \pm 1.662	35.978 \pm 0.140 \pm 0.653 \pm 1.709	36.344 \pm 0.112 \pm 0.546 \pm 1.558	35.023 \pm 0.103 \pm 0.550 \pm 1.541	33.970 \pm 0.095 \pm 0.659 \pm 1.413
(2.5,3.0)	26.858 \pm 0.227 \pm 0.865 \pm 1.295	28.324 \pm 0.109 \pm 0.440 \pm 1.250	27.658 \pm 0.089 \pm 0.358 \pm 1.336	26.622 \pm 0.080 \pm 0.554 \pm 1.151	24.771 \pm 0.095 \pm 0.536 \pm 1.062
(3.0,3.5)	19.321 \pm 0.165 \pm 0.615 \pm 0.963	19.133 \pm 0.155 \pm 0.295 \pm 0.817	19.185 \pm 0.062 \pm 0.381 \pm 0.828	18.717 \pm 0.069 \pm 0.251 \pm 0.822	17.124 \pm 0.076 \pm 0.345 \pm 0.737
(3.5,4.0)	12.973 \pm 0.114 \pm 0.409 \pm 0.563	13.543 \pm 0.057 \pm 0.282 \pm 0.578	13.060 \pm 0.059 \pm 0.336 \pm 0.672	12.918 \pm 0.057 \pm 0.354 \pm 0.542	12.153 \pm 0.056 \pm 0.248 \pm 0.531
(4.0,4.5)	9.619 \pm 0.098 \pm 0.379 \pm 0.449	9.947 \pm 0.120 \pm 0.222 \pm 0.432	9.450 \pm 0.055 \pm 0.189 \pm 0.405	8.918 \pm 0.057 \pm 0.234 \pm 0.386	8.350 \pm 0.038 \pm 0.205 \pm 0.360
(4.5,5.0)	6.639 \pm 0.075 \pm 0.323 \pm 0.341	7.358 \pm 0.039 \pm 0.205 \pm 0.323	6.747 \pm 0.036 \pm 0.137 \pm 0.292	6.269 \pm 0.042 \pm 0.170 \pm 0.267	5.691 \pm 0.036 \pm 0.145 \pm 0.239
(5.0,5.5)	4.851 \pm 0.063 \pm 0.194 \pm 0.212	4.857 \pm 0.040 \pm 0.151 \pm 0.215	4.723 \pm 0.032 \pm 0.114 \pm 0.200	4.430 \pm 0.035 \pm 0.126 \pm 0.194	3.983 \pm 0.028 \pm 0.105 \pm 0.177
(5.5,6.0)	3.492 \pm 0.051 \pm 0.163 \pm 0.148	3.726 \pm 0.027 \pm 0.088 \pm 0.168	3.437 \pm 0.029 \pm 0.088 \pm 0.146	3.142 \pm 0.025 \pm 0.121 \pm 0.132	2.877 \pm 0.022 \pm 0.087 \pm 0.130
(6.0,7.0)	2.230 \pm 0.023 \pm 0.104 \pm 0.099	2.275 \pm 0.022 \pm 0.058 \pm 0.097	2.196 \pm 0.019 \pm 0.061 \pm 0.097	1.964 \pm 0.014 \pm 0.053 \pm 0.086	1.842 \pm 0.013 \pm 0.049 \pm 0.081
(7.0,8.0)	1.395 \pm 0.021 \pm 0.063 \pm 0.060	1.297 \pm 0.013 \pm 0.037 \pm 0.056	1.161 \pm 0.014 \pm 0.044 \pm 0.050	1.188 \pm 0.009 \pm 0.049 \pm 0.053	1.052 \pm 0.009 \pm 0.032 \pm 0.048
(8.0,9.0)	0.818 \pm 0.013 \pm 0.022 \pm 0.036	0.764 \pm 0.010 \pm 0.018 \pm 0.032	0.702 \pm 0.008 \pm 0.014 \pm 0.031	0.682 \pm 0.008 \pm 0.022 \pm 0.031	0.605 \pm 0.007 \pm 0.015 \pm 0.028
(9.0,10.0)	0.438 \pm 0.019 \pm 0.032 \pm 0.020	0.446 \pm 0.007 \pm 0.009 \pm 0.019	0.394 \pm 0.006 \pm 0.012 \pm 0.018	0.428 \pm 0.006 \pm 0.010 \pm 0.020	0.355 \pm 0.006 \pm 0.009 \pm 0.018
(10.0,11.0)	0.284 \pm 0.016 \pm 0.015 \pm 0.013	0.278 \pm 0.007 \pm 0.010 \pm 0.012	0.239 \pm 0.005 \pm 0.007 \pm 0.028	0.276 \pm 0.005 \pm 0.008 \pm 0.014	0.227 \pm 0.005 \pm 0.008 \pm 0.012
(11.0,12.0)	0.196 \pm 0.009 \pm 0.008 \pm 0.008	0.168 \pm 0.005 \pm 0.007 \pm 0.008	0.145 \pm 0.004 \pm 0.005 \pm 0.007	0.184 \pm 0.005 \pm 0.009 \pm 0.011	0.143 \pm 0.005 \pm 0.006 \pm 0.008
(12.0,13.0)	0.136 \pm 0.005 \pm 0.006 \pm 0.006	0.103 \pm 0.005 \pm 0.008 \pm 0.005	0.098 \pm 0.003 \pm 0.004 \pm 0.005	0.116 \pm 0.004 \pm 0.006 \pm 0.007	0.110 \pm 0.004 \pm 0.006 \pm 0.006
(13.0,15.0)	0.074 \pm 0.004 \pm 0.004 \pm 0.004	0.055 \pm 0.002 \pm 0.003 \pm 0.002	0.053 \pm 0.002 \pm 0.002 \pm 0.003	0.069 \pm 0.002 \pm 0.003 \pm 0.005	0.059 \pm 0.003 \pm 0.004 \pm 0.004
(15.0,30.0)	(9.1 \pm 0.5 \pm 0.5 \pm 0.5) \times 10 ⁻³	(6.8 \pm 0.3 \pm 0.3 \pm 0.3) \times 10 ⁻³	(7.4 \pm 0.3 \pm 0.4 \pm 0.8) \times 10 ⁻³	(10.7 \pm 0.5 \pm 0.7 \pm 0.9) \times 10 ⁻³	(9.3 \pm 1.1 \pm 1.3 \pm 0.7) \times 10 ⁻³
p_T [GeV/c]\ y^*	(2.75, 3.00)	(3.00, 3.25)	(3.25, 3.50)	(3.50, 3.75)	(3.75, 4.00)
(0.0,1.0)	26.300 \pm 0.149 \pm 0.840 \pm 1.169	26.038 \pm 0.083 \pm 0.662 \pm 1.191	24.968 \pm 0.147 \pm 1.061 \pm 1.189	23.157 \pm 0.196 \pm 1.842 \pm 1.157	20.817 \pm 1.548 \pm 1.918 \pm 1.093
(1.0,1.5)	44.909 \pm 0.177 \pm 1.057 \pm 1.965	44.107 \pm 0.152 \pm 0.649 \pm 1.959	39.851 \pm 0.269 \pm 2.554 \pm 1.807	36.184 \pm 0.336 \pm 1.706 \pm 1.688	35.092 \pm 0.401 \pm 1.848 \pm 1.984
(1.5,2.0)	41.222 \pm 0.124 \pm 1.261 \pm 1.769	37.934 \pm 0.172 \pm 0.827 \pm 1.668	36.200 \pm 0.203 \pm 1.124 \pm 1.708	32.475 \pm 0.262 \pm 1.177 \pm 1.541	27.126 \pm 0.421 \pm 1.168 \pm 1.492
(2.0,2.5)	31.966 \pm 0.121 \pm 0.963 \pm 1.501	28.923 \pm 0.127 \pm 0.644 \pm 1.291	27.061 \pm 0.139 \pm 0.855 \pm 1.342	23.492 \pm 0.139 \pm 0.796 \pm 1.048	20.558 \pm 0.243 \pm 1.053 \pm 1.147
(2.5,3.0)	22.247 \pm 0.087 \pm 0.451 \pm 0.977	20.647 \pm 0.087 \pm 0.412 \pm 0.918	18.474 \pm 0.097 \pm 0.814 \pm 0.812	16.646 \pm 0.123 \pm 0.755 \pm 0.779	14.379 \pm 0.208 \pm 0.637 \pm 0.811
(3.0,3.5)	15.693 \pm 0.070 \pm 0.332 \pm 0.708	14.210 \pm 0.066 \pm 0.308 \pm 0.631	12.554 \pm 0.072 \pm 0.365 \pm 0.573	11.648 \pm 0.101 \pm 0.451 \pm 0.563	9.117 \pm 0.152 \pm 0.424 \pm 0.501
(3.5,4.0)	10.468 \pm 0.052 \pm 0.246 \pm 0.459	9.542 \pm 0.048 \pm 0.260 \pm 0.425	8.336 \pm 0.055 \pm 0.285 \pm 0.370	7.540 \pm 0.072 \pm 0.303 \pm 0.409	6.285 \pm 0.185 \pm 0.525 \pm 0.406
(4.0,4.5)	7.317 \pm 0.038 \pm 0.159 \pm 0.317	6.576 \pm 0.037 \pm 0.174 \pm 0.304	5.675 \pm 0.043 \pm 0.155 \pm 0.258	5.108 \pm 0.068 \pm 0.204 \pm 0.253	3.678 \pm 0.138 \pm 0.273 \pm 0.219
(4.5,5.0)	5.108 \pm 0.030 \pm 0.116 \pm 0.234	4.799 \pm 0.033 \pm 0.136 \pm 0.216	4.029 \pm 0.040 \pm 0.121 \pm 0.188	3.322 \pm 0.061 \pm 0.149 \pm 0.167	1.971 \pm 0.154 \pm 0.269 \pm 0.139
(5.0,5.5)	3.645 \pm 0.025 \pm 0.088 \pm 0.166	3.189 \pm 0.026 \pm 0.081 \pm 0.147	2.725 \pm 0.034 \pm 0.108 \pm 0.139	2.307 \pm 0.082 \pm 0.158 \pm 0.119	-
(5.5,6.0)	2.611 \pm 0.021 \pm 0.074 \pm 0.114	2.296 \pm 0.024 \pm 0.068 \pm 0.111	1.847 \pm 0.030 \pm 0.077 \pm 0.093	1.510 \pm 0.094 \pm 0.152 \pm 0.080	-
(6.0,7.0)	1.656 \pm 0.013 \pm 0.052 \pm 0.073	1.372 \pm 0.014 \pm 0.056 \pm 0.064	0.983 \pm 0.023 \pm 0.049 \pm 0.049	0.717 \pm 0.073 \pm 0.180 \pm 0.039	-
(7.0,8.0)	0.924 \pm 0.010 \pm 0.033 \pm 0.042	0.746 \pm 0.012 \pm 0.034 \pm 0.035	0.493 \pm 0.021 \pm 0.044 \pm 0.030	-	-
(8.0,9.0)	0.533 \pm 0.009 \pm 0.018 \pm 0.025	0.405 \pm 0.014 \pm 0.025 \pm 0.021	0.202 \pm 0.028 \pm 0.038 \pm 0.011	-	-
(9.0,10.0)	0.287 \pm 0.008 \pm 0.010 \pm 0.014	0.243 \pm 0.013 \pm 0.018 \pm 0.013	-	-	-
(10.0,11.0)	0.161 \pm 0.007 \pm 0.011 \pm 0.008	0.129 \pm 0.015 \pm 0.024 \pm 0.008	-	-	-
(11.0,12.0)	0.110 \pm 0.008 \pm 0.009 \pm 0.007	-	-	-	-
(12.0,13.0)	0.079 \pm 0.007 \pm 0.011 \pm 0.005	-	-	-	-
(13.0,15.0)	0.051 \pm 0.009 \pm 0.017 \pm 0.004	-	-	-	-
(15.0,30.0)	-	-	-	-	-

Table 3: Double-differential cross-sections for prompt D^0 mesons in intervals of p_T and y^* in backward rapidity regions. The first uncertainty is statistical, the second is the component of the systematic uncertainty that is uncorrelated across intervals and the third is the correlated component.

p_T [GeV/c]\(<y^*\)< th=""><th>(-2.75, -2.50)</th><th>(-3.00, -2.75)</th><th>(-3.25, -3.00)</th><th>(-3.50, -3.25)</th><th>(-3.75, -3.50)</th></y^*\)<>	(-2.75, -2.50)	(-3.00, -2.75)	(-3.25, -3.00)	(-3.50, -3.25)	(-3.75, -3.50)
(0,0,1,0)	26.423 \pm 0.077 \pm 1.135 \pm 2.046	30.978 \pm 0.110 \pm 0.658 \pm 2.272	31.059 \pm 0.086 \pm 0.746 \pm 1.764	32.488 \pm 0.079 \pm 0.575 \pm 1.859	30.706 \pm 0.075 \pm 0.555 \pm 1.731
(1,0,1,5)	50.258 \pm 0.329 \pm 1.766 \pm 3.570	55.180 \pm 0.193 \pm 1.433 \pm 3.295	56.266 \pm 0.152 \pm 1.055 \pm 3.169	55.760 \pm 0.139 \pm 0.959 \pm 2.935	53.809 \pm 0.143 \pm 0.971 \pm 2.852
(1,5,2,0)	51.254 \pm 0.277 \pm 1.579 \pm 3.222	51.164 \pm 0.162 \pm 0.940 \pm 2.918	52.039 \pm 0.133 \pm 1.058 \pm 2.768	50.232 \pm 0.125 \pm 0.751 \pm 2.968	47.612 \pm 0.121 \pm 1.373 \pm 2.535
(2,0,2,5)	41.615 \pm 0.211 \pm 1.109 \pm 2.506	42.476 \pm 0.126 \pm 1.047 \pm 2.332	41.267 \pm 0.099 \pm 0.490 \pm 2.482	39.322 \pm 0.092 \pm 0.618 \pm 2.022	36.252 \pm 0.094 \pm 1.045 \pm 1.873
(2,5,3,0)	27.597 \pm 0.140 \pm 0.693 \pm 1.672	29.397 \pm 0.089 \pm 0.468 \pm 1.603	29.188 \pm 0.150 \pm 0.490 \pm 1.570	27.301 \pm 0.062 \pm 0.725 \pm 1.417	24.672 \pm 0.080 \pm 0.394 \pm 1.389
(3,0,3,5)	20.272 \pm 0.106 \pm 0.478 \pm 1.148	20.175 \pm 0.079 \pm 0.294 \pm 1.079	20.078 \pm 0.055 \pm 0.590 \pm 1.055	18.466 \pm 0.049 \pm 0.464 \pm 0.946	16.460 \pm 0.056 \pm 0.292 \pm 0.805
(3,5,4,0)	13.875 \pm 0.078 \pm 0.362 \pm 0.737	13.732 \pm 0.046 \pm 0.269 \pm 0.727	13.085 \pm 0.079 \pm 0.394 \pm 0.678	12.130 \pm 0.046 \pm 0.221 \pm 0.637	10.876 \pm 0.041 \pm 0.303 \pm 0.544
(4,0,4,5)	9.523 \pm 0.109 \pm 0.258 \pm 0.517	9.049 \pm 0.040 \pm 0.232 \pm 0.515	8.776 \pm 0.039 \pm 0.182 \pm 0.488	8.053 \pm 0.034 \pm 0.160 \pm 0.407	6.978 \pm 0.032 \pm 0.145 \pm 0.359
(4,5,5,0)	6.647 \pm 0.044 \pm 0.182 \pm 0.363	6.474 \pm 0.043 \pm 0.190 \pm 0.325	6.065 \pm 0.028 \pm 0.132 \pm 0.294	5.284 \pm 0.026 \pm 0.124 \pm 0.269	4.464 \pm 0.022 \pm 0.105 \pm 0.216
(5,0,5,5)	4.622 \pm 0.035 \pm 0.153 \pm 0.247	4.353 \pm 0.032 \pm 0.106 \pm 0.228	3.888 \pm 0.030 \pm 0.093 \pm 0.202	3.662 \pm 0.023 \pm 0.089 \pm 0.184	3.006 \pm 0.019 \pm 0.091 \pm 0.150
(5,5,6,0)	3.160 \pm 0.041 \pm 0.115 \pm 0.172	2.878 \pm 0.028 \pm 0.089 \pm 0.158	2.741 \pm 0.024 \pm 0.086 \pm 0.133	2.454 \pm 0.017 \pm 0.068 \pm 0.125	2.209 \pm 0.016 \pm 0.064 \pm 0.114
(6,0,7,0)	1.893 \pm 0.023 \pm 0.098 \pm 0.105	1.798 \pm 0.015 \pm 0.044 \pm 0.094	1.669 \pm 0.012 \pm 0.047 \pm 0.084	1.478 \pm 0.010 \pm 0.037 \pm 0.087	1.225 \pm 0.009 \pm 0.039 \pm 0.066
(7,0,8,0)	1.021 \pm 0.012 \pm 0.034 \pm 0.055	1.055 \pm 0.007 \pm 0.030 \pm 0.054	0.807 \pm 0.009 \pm 0.027 \pm 0.044	0.824 \pm 0.007 \pm 0.026 \pm 0.054	0.646 \pm 0.006 \pm 0.021 \pm 0.039
(8,0,9,0)	0.632 \pm 0.014 \pm 0.014 \pm 0.033	0.562 \pm 0.006 \pm 0.020 \pm 0.029	0.467 \pm 0.006 \pm 0.011 \pm 0.029	0.429 \pm 0.005 \pm 0.008 \pm 0.030	0.355 \pm 0.005 \pm 0.010 \pm 0.022
(9,0,10,0)	0.377 \pm 0.006 \pm 0.010 \pm 0.019	0.312 \pm 0.006 \pm 0.008 \pm 0.017	0.266 \pm 0.005 \pm 0.007 \pm 0.017	0.256 \pm 0.004 \pm 0.007 \pm 0.020	0.194 \pm 0.004 \pm 0.006 \pm 0.013
(10,0,11,0)	0.241 \pm 0.005 \pm 0.008 \pm 0.013	0.184 \pm 0.003 \pm 0.006 \pm 0.011	0.151 \pm 0.003 \pm 0.004 \pm 0.011	0.157 \pm 0.003 \pm 0.005 \pm 0.014	0.117 \pm 0.003 \pm 0.008 \pm 0.009
(11,0,12,0)	0.155 \pm 0.009 \pm 0.007 \pm 0.008	0.118 \pm 0.006 \pm 0.006 \pm 0.008	0.102 \pm 0.003 \pm 0.004 \pm 0.010	0.092 \pm 0.003 \pm 0.004 \pm 0.011	0.080 \pm 0.003 \pm 0.005 \pm 0.006
(12,0,13,0)	0.093 \pm 0.003 \pm 0.007 \pm 0.006	0.080 \pm 0.003 \pm 0.004 \pm 0.010	0.067 \pm 0.002 \pm 0.004 \pm 0.008	0.067 \pm 0.002 \pm 0.003 \pm 0.008	0.041 \pm 0.002 \pm 0.004 \pm 0.004
(13,0,15,0)	0.056 \pm 0.002 \pm 0.002 \pm 0.005	0.046 \pm 0.002 \pm 0.003 \pm 0.012	0.033 \pm 0.001 \pm 0.001 \pm 0.005	0.033 \pm 0.002 \pm 0.002 \pm 0.005	0.024 \pm 0.002 \pm 0.003 \pm 0.002
(15,0,30,0)	(8.6 \pm 0.3 \pm 0.6 \pm 2.4) \times 10 ⁻³	(5.5 \pm 0.2 \pm 0.4 \pm 1.5) \times 10 ⁻³	(4.6 \pm 0.2 \pm 0.3 \pm 0.9) \times 10 ⁻³	(6.1 \pm 0.4 \pm 0.6 \pm 1.1) \times 10 ⁻³	
p_T [GeV/c]\(<y^*\)< th=""><th>(-4,0,0)</th><th>(-4,25, -3,75)</th><th>(-4,25, -4,00)</th><th>(-4,50, -4,25)</th><th>(-4,75, -4,50)</th></y^*\)<>	(-4,0,0)	(-4,25, -3,75)	(-4,25, -4,00)	(-4,50, -4,25)	(-4,75, -4,50)
(0,0,1,0)	30.648 \pm 0.072 \pm 0.728 \pm 1.785	30.899 \pm 0.087 \pm 0.480 \pm 1.646	30.195 \pm 0.102 \pm 1.591 \pm 1.724	27.540 \pm 0.167 \pm 2.236 \pm 1.559	27.064 \pm 0.176 \pm 1.855 \pm 1.897
(1,0,1,5)	50.516 \pm 0.149 \pm 1.295 \pm 2.628	49.920 \pm 0.154 \pm 1.026 \pm 2.753	45.676 \pm 0.273 \pm 1.648 \pm 2.581	39.963 \pm 0.244 \pm 1.630 \pm 2.396	37.309 \pm 0.360 \pm 2.581 \pm 2.781
(1,5,2,0)	46.320 \pm 0.125 \pm 1.204 \pm 2.395	42.339 \pm 0.125 \pm 1.000 \pm 2.246	36.955 \pm 0.155 \pm 1.076 \pm 2.017	33.341 \pm 0.208 \pm 0.936 \pm 2.091	29.194 \pm 0.518 \pm 1.784 \pm 2.086
(2,0,2,5)	33.509 \pm 0.107 \pm 0.558 \pm 1.718	30.329 \pm 0.102 \pm 0.515 \pm 1.557	27.392 \pm 0.119 \pm 0.550 \pm 1.415	22.942 \pm 0.159 \pm 0.702 \pm 1.405	19.056 \pm 0.326 \pm 1.006 \pm 1.649
(2,5,3,0)	21.950 \pm 0.069 \pm 0.390 \pm 1.114	20.166 \pm 0.078 \pm 0.350 \pm 1.076	17.099 \pm 0.093 \pm 0.526 \pm 1.266	13.958 \pm 0.096 \pm 0.359 \pm 0.918	10.073 \pm 0.161 \pm 0.579 \pm 0.860
(3,0,3,5)	14.270 \pm 0.055 \pm 0.262 \pm 0.720	12.183 \pm 0.054 \pm 0.235 \pm 0.681	10.923 \pm 0.060 \pm 0.233 \pm 0.656	8.404 \pm 0.075 \pm 0.256 \pm 0.580	5.923 \pm 0.129 \pm 0.373 \pm 0.566
(3,5,4,0)	9.224 \pm 0.037 \pm 0.187 \pm 0.462	8.029 \pm 0.040 \pm 0.239 \pm 0.453	6.325 \pm 0.044 \pm 0.186 \pm 0.394	4.711 \pm 0.058 \pm 0.172 \pm 0.368	3.459 \pm 0.169 \pm 0.395 \pm 0.339
(4,0,4,5)	5.943 \pm 0.029 \pm 0.119 \pm 0.306	4.791 \pm 0.028 \pm 0.114 \pm 0.295	4.084 \pm 0.035 \pm 0.116 \pm 0.272	2.899 \pm 0.050 \pm 0.177 \pm 0.231	1.790 \pm 0.116 \pm 0.282 \pm 0.188
(4,5,5,0)	3.863 \pm 0.026 \pm 0.098 \pm 0.208	3.150 \pm 0.024 \pm 0.094 \pm 0.196	2.502 \pm 0.030 \pm 0.088 \pm 0.165	1.621 \pm 0.048 \pm 0.135 \pm 0.142	
(5,0,5,5)	2.708 \pm 0.019 \pm 0.076 \pm 0.154	1.993 \pm 0.019 \pm 0.070 \pm 0.131	1.598 \pm 0.025 \pm 0.082 \pm 0.122	1.001 \pm 0.072 \pm 0.117 \pm 0.093	
(5,5,6,0)	1.722 \pm 0.015 \pm 0.053 \pm 0.098	1.389 \pm 0.016 \pm 0.052 \pm 0.087	0.895 \pm 0.021 \pm 0.058 \pm 0.066	0.458 \pm 0.049 \pm 0.086 \pm 0.040	
(6,0,7,0)	0.945 \pm 0.008 \pm 0.031 \pm 0.063	0.736 \pm 0.010 \pm 0.027 \pm 0.054	0.550 \pm 0.023 \pm 0.048 \pm 0.046		
(7,0,8,0)	0.489 \pm 0.007 \pm 0.020 \pm 0.032	0.371 \pm 0.010 \pm 0.026 \pm 0.028	0.241 \pm 0.023 \pm 0.053 \pm 0.024		
(8,0,9,0)	0.258 \pm 0.005 \pm 0.009 \pm 0.018	0.153 \pm 0.010 \pm 0.011 \pm 0.012			
(9,0,10,0)	0.128 \pm 0.006 \pm 0.007 \pm 0.010	0.083 \pm 0.013 \pm 0.014 \pm 0.007			
(10,0,11,0)	0.069 \pm 0.004 \pm 0.006 \pm 0.006				
(11,0,12,0)	0.033 \pm 0.004 \pm 0.005 \pm 0.003				
(12,0,13,0)					
(13,0,15,0)					
(15,0,30,0)					

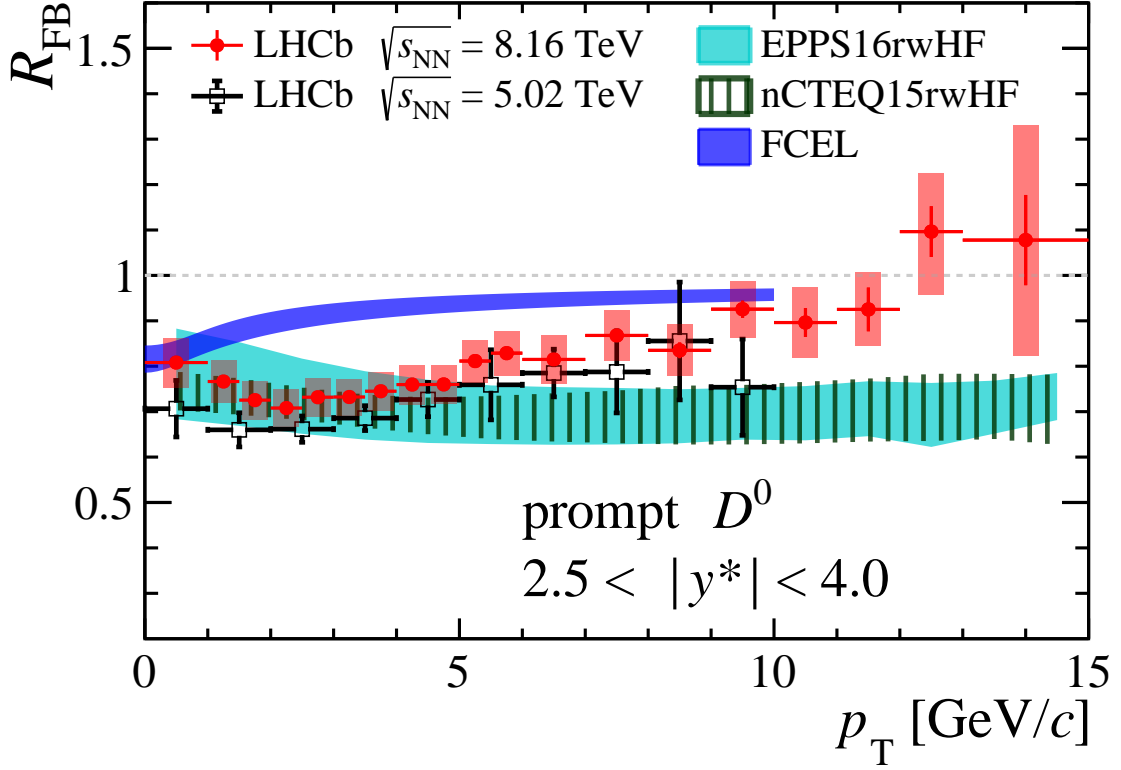


Figure 9: Forward-backward production ratio for prompt D^0 mesons as a function of p_T , integrated over the common rapidity range $2.5 < |y^*| < 4.0$. The error bars show the statistical uncertainties and the boxes show the systematic uncertainties. The LHCb results at $\sqrt{s_{NN}} = 5.02$ TeV [14] and theoretical calculations at $\sqrt{s_{NN}} = 8.16$ TeV from Refs. [9, 64, 65] are also shown. For the LHCb results at $\sqrt{s_{NN}} = 5.02$ TeV, the error bars show the quadratic sum of statistical and systematic uncertainties.

Table 4: Nuclear modification factor $R_{p\text{Pb}}$ for prompt D^0 mesons in intervals of p_T and y^* for $p_T < 10 \text{ GeV}/c$. The first uncertainty is statistical and the second is the systematic.

$p_T [\text{GeV}/c] \setminus y^*$	(2.5, 4.0)	(2.0, 2.5)	(2.5, 3.0)	(3.0, 3.5)	(3.5, 4.0)
(0.0,1.0)	$0.546 \pm 0.002 \pm 0.033$	$0.485 \pm 0.001 \pm 0.041$	$0.525 \pm 0.001 \pm 0.032$	$0.556 \pm 0.002 \pm 0.036$	$0.561 \pm 0.005 \pm 0.039$
(1.0,2.0)	$0.596 \pm 0.002 \pm 0.034$	$0.557 \pm 0.001 \pm 0.037$	$0.591 \pm 0.003 \pm 0.034$	$0.611 \pm 0.002 \pm 0.036$	$0.585 \pm 0.003 \pm 0.038$
(2.0,3.0)	$0.637 \pm 0.001 \pm 0.034$	$0.648 \pm 0.001 \pm 0.036$	$0.637 \pm 0.001 \pm 0.034$	$0.648 \pm 0.001 \pm 0.035$	$0.624 \pm 0.003 \pm 0.037$
(3.0,4.0)	$0.671 \pm 0.001 \pm 0.036$	$0.679 \pm 0.001 \pm 0.038$	$0.676 \pm 0.002 \pm 0.035$	$0.673 \pm 0.002 \pm 0.036$	$0.659 \pm 0.004 \pm 0.044$
(4.0,5.0)	$0.706 \pm 0.002 \pm 0.040$	$0.697 \pm 0.002 \pm 0.042$	$0.719 \pm 0.002 \pm 0.039$	$0.710 \pm 0.003 \pm 0.041$	$0.681 \pm 0.007 \pm 0.048$
(5.0,6.0)	$0.719 \pm 0.005 \pm 0.048$	$0.718 \pm 0.003 \pm 0.056$	$0.722 \pm 0.002 \pm 0.047$	$0.737 \pm 0.004 \pm 0.047$	$0.688 \pm 0.019 \pm 0.064$
(6.0,7.0)	$0.710 \pm 0.014 \pm 0.067$	$0.721 \pm 0.004 \pm 0.056$	$0.769 \pm 0.004 \pm 0.058$	$0.725 \pm 0.006 \pm 0.057$	$0.568 \pm 0.061 \pm 0.169$
(7.0,8.0)	$0.752 \pm 0.005 \pm 0.061$	$0.777 \pm 0.006 \pm 0.067$	$0.783 \pm 0.005 \pm 0.061$	$0.709 \pm 0.010 \pm 0.067$	-
(8.0,9.0)	$0.768 \pm 0.011 \pm 0.073$	$0.717 \pm 0.006 \pm 0.084$	$0.832 \pm 0.008 \pm 0.074$	$0.683 \pm 0.023 \pm 0.078$	-
(9.0,10.0)	$0.784 \pm 0.018 \pm 0.111$	$0.687 \pm 0.007 \pm 0.070$	$0.764 \pm 0.011 \pm 0.086$	$0.814 \pm 0.043 \pm 0.160$	-

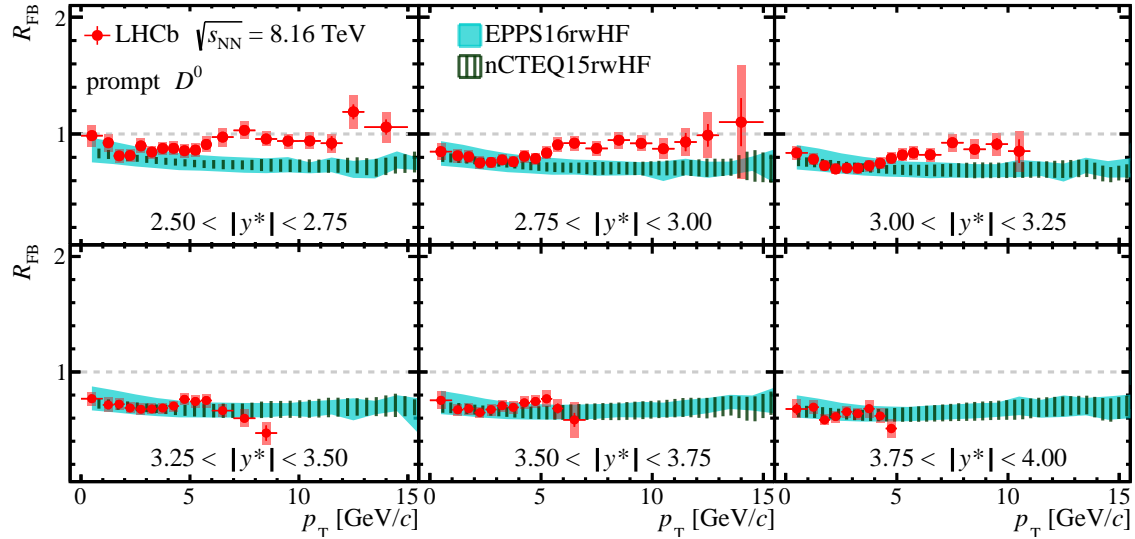


Figure 10: Forward and backward production ratio R_{FB} for prompt D^0 mesons as a function of p_T in different $|y^*|$ intervals. The error bars show the statistical uncertainties and the boxes show the systematic uncertainties. The theoretical calculations from Refs. [64, 65] are also shown.

Table 5: Nuclear modification factor $R_{p\text{Pb}}$ for prompt D^0 mesons in intervals of p_T and y^* for $p_T < 10 \text{ GeV}/c$. The first uncertainty is statistical and the second is systematic.

$p_T [\text{GeV}/c] \setminus y^*$	(-4.0, -2.5)	(-3.0, -2.5)	(-3.5, -3.0)	(-4.0, -3.5)	(-4.5, -4.0)
(0.0,1.0)	$0.691 \pm 0.001 \pm 0.049$	$0.607 \pm 0.002 \pm 0.047$	$0.706 \pm 0.001 \pm 0.049$	$0.781 \pm 0.001 \pm 0.054$	$0.959 \pm 0.002 \pm 0.080$
(1.0,2.0)	$0.803 \pm 0.001 \pm 0.053$	$0.718 \pm 0.001 \pm 0.052$	$0.824 \pm 0.001 \pm 0.054$	$0.891 \pm 0.001 \pm 0.057$	$0.994 \pm 0.002 \pm 0.068$
(2.0,3.0)	$0.891 \pm 0.001 \pm 0.056$	$0.804 \pm 0.002 \pm 0.056$	$0.940 \pm 0.002 \pm 0.056$	$0.960 \pm 0.001 \pm 0.058$	$1.087 \pm 0.002 \pm 0.075$
(3.0,4.0)	$0.917 \pm 0.001 \pm 0.053$	$0.841 \pm 0.003 \pm 0.051$	$0.982 \pm 0.002 \pm 0.056$	$0.952 \pm 0.002 \pm 0.057$	$1.134 \pm 0.003 \pm 0.099$
(4.0,5.0)	$0.916 \pm 0.003 \pm 0.056$	$0.860 \pm 0.008 \pm 0.054$	$0.962 \pm 0.002 \pm 0.058$	$0.948 \pm 0.003 \pm 0.062$	$1.031 \pm 0.004 \pm 0.139$
(5.0,6.0)	$0.894 \pm 0.002 \pm 0.062$	$0.832 \pm 0.005 \pm 0.061$	$0.929 \pm 0.003 \pm 0.060$	$0.956 \pm 0.004 \pm 0.072$	$1.493 \pm 0.010 \pm 0.403$
(6.0,7.0)	$0.884 \pm 0.003 \pm 0.074$	$0.819 \pm 0.005 \pm 0.064$	$0.911 \pm 0.005 \pm 0.073$	$0.974 \pm 0.005 \pm 0.111$	-
(7.0,8.0)	$0.898 \pm 0.004 \pm 0.086$	$0.827 \pm 0.006 \pm 0.067$	$0.881 \pm 0.006 \pm 0.084$	$1.101 \pm 0.009 \pm 0.158$	-
(8.0,9.0)	$0.918 \pm 0.006 \pm 0.118$	$0.861 \pm 0.010 \pm 0.079$	$0.857 \pm 0.008 \pm 0.091$	$1.197 \pm 0.014 \pm 0.352$	-
(9.0,10.0)	$0.867 \pm 0.007 \pm 0.123$	$0.805 \pm 0.010 \pm 0.091$	$0.964 \pm 0.011 \pm 0.181$	-	-

Table 6: Forward-backward production ratio R_{FB} for prompt D^0 mesons as a function of p_{T} , integrated over $2.5 < |y^*| < 4.0$. The first uncertainty is statistical, the second is the component of the systematic uncertainty that is uncorrelated across intervals and the third is the correlated component.

$p_{\text{T}} [\text{GeV}/c]$	R_{FB}
(0.0,1.0)	$0.808 \pm 0.009 \pm 0.019 \pm 0.051$
(1.0,1.5)	$0.766 \pm 0.002 \pm 0.014 \pm 0.044$
(1.5,2.0)	$0.725 \pm 0.002 \pm 0.011 \pm 0.041$
(2.0,2.5)	$0.708 \pm 0.002 \pm 0.011 \pm 0.039$
(2.5,3.0)	$0.732 \pm 0.002 \pm 0.011 \pm 0.040$
(3.0,3.5)	$0.732 \pm 0.002 \pm 0.011 \pm 0.039$
(3.5,4.0)	$0.745 \pm 0.003 \pm 0.013 \pm 0.040$
(4.0,4.5)	$0.760 \pm 0.004 \pm 0.012 \pm 0.042$
(4.5,5.0)	$0.760 \pm 0.006 \pm 0.015 \pm 0.040$
(5.0,5.5)	$0.811 \pm 0.006 \pm 0.016 \pm 0.044$
(5.5,6.0)	$0.829 \pm 0.009 \pm 0.020 \pm 0.045$
(6.0,7.0)	$0.815 \pm 0.010 \pm 0.029 \pm 0.045$
(7.0,8.0)	$0.868 \pm 0.008 \pm 0.024 \pm 0.051$
(8.0,9.0)	$0.835 \pm 0.017 \pm 0.027 \pm 0.050$
(9.0,10.0)	$0.926 \pm 0.019 \pm 0.028 \pm 0.055$
(10.0,11.0)	$0.896 \pm 0.032 \pm 0.050 \pm 0.060$
(11.0,12.0)	$0.925 \pm 0.048 \pm 0.051 \pm 0.063$
(12.0,13.0)	$1.096 \pm 0.056 \pm 0.088 \pm 0.106$
(13.0,15.0)	$1.078 \pm 0.099 \pm 0.178 \pm 0.181$

Acknowledgements

We express our gratitude to our colleagues in the CERN accelerator departments for the excellent performance of the LHC. We thank the technical and administrative staff at the LHCb institutes. We acknowledge support from CERN and from the national agencies: CAPES, CNPq, FAPERJ and FINEP (Brazil); MOST and NSFC (China); CNRS/IN2P3 (France); BMBF, DFG and MPG (Germany); INFN (Italy); NWO (Netherlands); MNiSW and NCN (Poland); MEN/IFA (Romania); MICINN (Spain); SNSF and SER (Switzerland); NASU (Ukraine); STFC (United Kingdom); DOE NP and NSF (USA). We acknowledge the computing resources that are provided by CERN, IN2P3 (France), KIT and DESY (Germany), INFN (Italy), SURF (Netherlands), PIC (Spain), GridPP (United Kingdom), CSCS (Switzerland), IFIN-HH (Romania), CBPF (Brazil), Polish WLCG (Poland) and NERSC (USA). We are indebted to the communities behind the multiple open-source software packages on which we depend. Individual groups or members have received support from ARC and ARDC (Australia); Minciencias (Colombia); AvH Foundation (Germany); EPLANET, Marie Skłodowska-Curie Actions and ERC (European Union); A*MIDEX, ANR, IPhU and Labex P2IO, and Région Auvergne-Rhône-Alpes (France); Key Research Program of Frontier Sciences of CAS, CAS PIFI, CAS CCEPP, Fundamental Research Funds for the Central Universities, and Sci. & Tech. Program of Guangzhou (China); GVA, XuntaGal, GENCAT and Prog. Atracción Talento, CM (Spain); SRC (Sweden); the Leverhulme Trust, the Royal Society and UKRI (United Kingdom).

References

- [1] K. Yagi, T. Hatsuda, and Y. Miake, *Quark-gluon plasma: From big bang to little bang*, vol. 23, Cambridge University Press, 2005.
- [2] K. J. Eskola, H. Paukkunen, and C. A. Salgado, *EPS09: A new generation of NLO and LO nuclear parton distribution functions*, JHEP **04** (2009) 065, [arXiv:0902.4154](https://arxiv.org/abs/0902.4154).
- [3] D. de Florian and R. Sassot, *Nuclear parton distributions at next-to-leading order*, Phys. Rev. **D69** (2004) 074028, [arXiv:hep-ph/0311227](https://arxiv.org/abs/hep-ph/0311227).
- [4] M. Hirai, S. Kumano, and T.-H. Nagai, *Determination of nuclear parton distribution functions and their uncertainties in next-to-leading order*, Phys. Rev. **C76** (2007) 065207, [arXiv:0709.3038](https://arxiv.org/abs/0709.3038).
- [5] N. Armesto, *Nuclear shadowing*, J. Phys. **G32** (2006) R367, [arXiv:hep-ph/0604108](https://arxiv.org/abs/hep-ph/0604108).
- [6] F. Gelis, E. Iancu, J. Jalilian-Marian, and R. Venugopalan, *The color glass condensate*, Ann. Rev. Nucl. Part. Sci. **60** (2010) 463, [arXiv:1002.0333](https://arxiv.org/abs/1002.0333).
- [7] I. Vitev, *Non-Abelian energy loss in cold nuclear matter*, Phys. Rev. **C75** (2007) 064906, [arXiv:hep-ph/0703002](https://arxiv.org/abs/hep-ph/0703002).
- [8] Z.-B. Kang *et al.*, *Multiple scattering effects on heavy meson production in p+A collisions at backward rapidity*, Phys. Lett. **B740** (2015) 23, [arXiv:1409.2494](https://arxiv.org/abs/1409.2494).
- [9] F. Arleo, G. Jackson, and S. Peigné, *Impact of fully coherent energy loss on heavy meson production in pA collisions*, JHEP **01** (2022) 164, [arXiv:2107.05871](https://arxiv.org/abs/2107.05871).

- [10] C. Zhang *et al.*, *Elliptic flow of heavy quarkonia in pA collisions*, Phys. Rev. Lett. **122** (2019) 172302, [arXiv:1901.10320](#).
- [11] W. Zhao *et al.*, *Probing the Partonic Degrees of Freedom in High-Multiplicity p–Pb collisions at $\sqrt{s_{NN}} = 5.02 \text{ TeV}$* , Phys. Rev. Lett. **125** (2020) 072301, [arXiv:1911.00826](#).
- [12] CMS collaboration, A. M. Sirunyan *et al.*, *Elliptic flow of charm and strange hadrons in high-multiplicity pPb collisions at $\sqrt{s_{NN}} = 8.16 \text{ TeV}$* , Phys. Rev. Lett. **121** (2018) 082301, [arXiv:1804.09767](#).
- [13] CMS collaboration, A. M. Sirunyan *et al.*, *Observation of prompt J/ψ meson elliptic flow in high-multiplicity pPb collisions at $\sqrt{s_{NN}} = 8.16 \text{ TeV}$* , Phys. Lett. **B791** (2019) 172, [arXiv:1810.01473](#).
- [14] LHCb collaboration, R. Aaij *et al.*, *Study of prompt D^0 meson production in pPb collisions at $\sqrt{s_{NN}} = 5 \text{ TeV}$* , JHEP **10** (2017) 090, [arXiv:1707.02750](#).
- [15] LHCb collaboration, R. Aaij *et al.*, *Prompt Λ_c^+ production in pPb collisions at $\sqrt{s_{NN}} = 5.02 \text{ TeV}$* , JHEP **02** (2019) 102, [arXiv:1809.01404](#).
- [16] LHCb collaboration, R. Aaij *et al.*, *Prompt and nonprompt J/ψ production and nuclear modification in pPb collisions at $\sqrt{s_{NN}} = 8.16 \text{ TeV}$* , Phys. Lett. **B774** (2017) 159, [arXiv:1706.07122](#).
- [17] LHCb collaboration, R. Aaij *et al.*, *Measurement of B^+ , B^0 and Λ_b^0 production in pPb collisions at $\sqrt{s_{NN}} = 8.16 \text{ TeV}$* , Phys. Rev. **D99** (2019) 052011, [arXiv:1902.05599](#).
- [18] LHCb collaboration, R. Aaij *et al.*, *Study of Υ production in pPb collisions at $\sqrt{s_{NN}} = 8.16 \text{ TeV}$* , JHEP **11** (2018) 194, [arXiv:1810.07655](#).
- [19] ALICE collaboration, B. B. Abelev *et al.*, *Measurement of prompt D-meson production in p – Pb collisions at $\sqrt{s_{NN}} = 5.02 \text{ TeV}$* , Phys. Rev. Lett. **113** (2014) 232301, [arXiv:1405.3452](#).
- [20] ALICE collaboration, J. Adam *et al.*, *Measurement of D-meson production versus multiplicity in p-Pb collisions at $\sqrt{s_{NN}} = 5.02 \text{ TeV}$* , JHEP **08** (2016) 078, [arXiv:1602.07240](#).
- [21] ALICE collaboration, J. Adam *et al.*, *D-meson production in p-Pb collisions at $\sqrt{s_{NN}} = 5.02 \text{ TeV}$ and in pp collisions at $\sqrt{s} = 7 \text{ TeV}$* , Phys. Rev. **C94** (2016) 054908, [arXiv:1605.07569](#).
- [22] ALICE collaboration, S. Acharya *et al.*, *Measurement of prompt D^0 , D^+ , D^{*+} , and D_s^+ production in p-Pb collisions at $\sqrt{s_{NN}} = 5.02 \text{ TeV}$* , JHEP **12** (2019) 092, [arXiv:1906.03425](#).
- [23] ALICE collaboration, S. Acharya *et al.*, *Λ_c^+ production and baryon-to-meson ratios in pp and p-Pb collisions at $\sqrt{s_{NN}} = 5.02 \text{ TeV}$ at the LHC*, Phys. Rev. Lett. **127** (2021) 202301, [arXiv:2011.06078](#).
- [24] ALICE collaboration, S. Acharya *et al.*, *Λ_c^+ production in pp and in p-Pb collisions at $\sqrt{s_{NN}} = 5.02 \text{ TeV}$* , Phys. Rev. **C104** (2021) 054905, [arXiv:2011.06079](#).

- [25] ALICE collaboration, S. Acharya *et al.*, *Production of muons from heavy-flavour hadron decays in p-Pb collisions at $\sqrt{s_{NN}} = 5.02 \text{ TeV}$* , Phys. Lett. **B770** (2017) 459, arXiv:1702.01479.
- [26] ALICE collaboration, S. Acharya *et al.*, *Measurement of nuclear effects on $\psi(2S)$ production in p-Pb collisions at $\sqrt{s_{NN}} = 8.16 \text{ TeV}$* , JHEP **07** (2020) 237, arXiv:2003.06053.
- [27] ALICE collaboration, S. Acharya *et al.*, *Υ production in p-Pb collisions at $\sqrt{s_{NN}} = 8.16 \text{ TeV}$* , Phys. Lett. **B806** (2020) 135486, arXiv:1910.14405.
- [28] ALICE collaboration, S. Acharya *et al.*, *Inclusive J/ψ production at forward and backward rapidity in p-Pb collisions at $\sqrt{s_{NN}} = 8.16 \text{ TeV}$* , JHEP **07** (2018) 160, arXiv:1805.04381.
- [29] ALICE collaboration, S. Acharya *et al.*, *Prompt and non-prompt J/ψ production and nuclear modification at mid-rapidity in p-Pb collisions at $\sqrt{s_{NN}} = 5.02 \text{ TeV}$* , Eur. Phys. J. **C78** (2018) 466, arXiv:1802.00765.
- [30] ALICE collaboration, B. B. Abelev *et al.*, *Production of inclusive $\Upsilon(1S)$ and $\Upsilon(2S)$ in p-Pb collisions at $\sqrt{s_{NN}} = 5.02 \text{ TeV}$* , Phys. Lett. **B740** (2015) 105, arXiv:1410.2234.
- [31] ATLAS collaboration, M. Aaboud *et al.*, *Measurement of quarkonium production in proton-lead and proton-proton collisions at 5.02 TeV with the ATLAS detector*, Eur. Phys. J. **C78** (2018) 171, arXiv:1709.03089.
- [32] CMS collaboration, A. Tumasyan *et al.*, *Nuclear modification of Υ states in pPb collisions at $\sqrt{s_{NN}} = 5.02 \text{ TeV}$* , Phys. Lett. **B835** (2022) 137397, arXiv:2202.11807.
- [33] CMS collaboration, A. M. Sirunyan *et al.*, *Measurement of prompt and nonprompt J/ψ production in pp and pPb collisions at $\sqrt{s_{NN}} = 5.02 \text{ TeV}$* , Eur. Phys. J. **C77** (2017) 269, arXiv:1702.01462.
- [34] CMS collaboration, V. Khachatryan *et al.*, *Study of B meson production in p+Pb collisions at $\sqrt{s_{NN}} = 5.02 \text{ TeV}$ using exclusive hadronic decays*, Phys. Rev. Lett. **116** (2016) 032301, arXiv:1508.06678.
- [35] CMS collaboration, A. M. Sirunyan *et al.*, *Measurements of the charm jet cross section and nuclear modification factor in pPb collisions at $\sqrt{s_{NN}} = 5.02 \text{ TeV}$* , Phys. Lett. **B772** (2017) 306, arXiv:1612.08972.
- [36] CMS collaboration, V. Khachatryan *et al.*, *Transverse momentum spectra of inclusive b jets in pPb collisions at $\sqrt{s_{NN}} = 5.02 \text{ TeV}$* , Phys. Lett. **B754** (2016) 59, arXiv:1510.03373.
- [37] STAR collaboration, J. Adams *et al.*, *Open charm yields in $d + Au$ collisions at $\sqrt{s_{NN}} = 200 \text{ GeV}$* , Phys. Rev. Lett. **94** (2005) 062301, arXiv:nucl-ex/0407006.
- [38] PHENIX collaboration, A. Adare *et al.*, *Cold-nuclear-matter effects on heavy-quark production in $d+Au$ collisions at $\sqrt{s_{NN}} = 200 \text{ GeV}$* , Phys. Rev. Lett. **109** (2012) 242301, arXiv:1208.1293.

- [39] K. J. Eskola, I. Helenius, P. Paakkinen, and H. Paukkunen, *A QCD analysis of LHCb D-meson data in p+Pb collisions*, JHEP **05** (2020) 037, [arXiv:1906.02512](#).
- [40] R. A. Khalek *et al.*, *nNNPDF3.0: Evidence for a modified partonic structure in heavy nuclei*, [arXiv:2201.12363](#).
- [41] LHCb collaboration, A. A. Alves Jr. *et al.*, *The LHCb detector at the LHC*, JINST **3** (2008) S08005.
- [42] LHCb collaboration, R. Aaij *et al.*, *LHCb detector performance*, Int. J. Mod. Phys. **A30** (2015) 1530022, [arXiv:1412.6352](#).
- [43] LHCb collaboration, R. Aaij *et al.*, *Precision luminosity measurements at LHCb*, JINST **9** (2014) P12005, [arXiv:1410.0149](#).
- [44] T. Sjöstrand, S. Mrenna, and P. Skands, *PYTHIA 6.4 physics and manual*, JHEP **05** (2006) 026, [arXiv:hep-ph/0603175](#); T. Sjöstrand, S. Mrenna, and P. Skands, *A brief introduction to PYTHIA 8.1*, Comput. Phys. Commun. **178** (2008) 852, [arXiv:0710.3820](#).
- [45] T. Pierog *et al.*, *EPOS LHC: Test of collective hadronization with data measured at the CERN Large Hadron Collider*, Phys. Rev. **C92** (2015) 034906.
- [46] I. Belyaev *et al.*, *Handling of the generation of primary events in Gauss, the LHCb simulation framework*, J. Phys. Conf. Ser. **331** (2011) 032047.
- [47] D. J. Lange, *The EvtGen particle decay simulation package*, Nucl. Instrum. Meth. **A462** (2001) 152.
- [48] P. Golonka and Z. Was, *PHOTOS Monte Carlo: A precision tool for QED corrections in Z and W decays*, Eur. Phys. J. **C45** (2006) 97, [arXiv:hep-ph/0506026](#).
- [49] Geant4 collaboration, J. Allison *et al.*, *Geant4 developments and applications*, IEEE Trans. Nucl. Sci. **53** (2006) 270; Geant4 collaboration, S. Agostinelli *et al.*, *Geant4: A simulation toolkit*, Nucl. Instrum. Meth. **A506** (2003) 250.
- [50] M. Clemencic *et al.*, *The LHCb simulation application, Gauss: Design, evolution and experience*, J. Phys. Conf. Ser. **331** (2011) 032023.
- [51] Particle Data Group, R. L. Workman *et al.*, *Review of Particle Physics*, PTEP **2022** (2022) 083C01.
- [52] T. Skwarnicki, *A study of the radiative cascade transitions between the Upsilon-prime and Upsilon resonances*, PhD thesis, Institute of Nuclear Physics, Krakow, 1986, DESY-F31-86-02.
- [53] M. Pivk and F. R. Le Diberder, *sPlot: A statistical tool to unfold data distributions*, Nucl. Instrum. Meth. **A555** (2005) 356, [arXiv:physics/0402083](#).
- [54] A. D. Bukin, *Fitting function for asymmetric peaks*, [arXiv:0711.4449](#).

- [55] See Supplemental Material at [link inserted by publisher] for a summary of systematic uncertainties and numerical results and additional plots for the fit result, nuclear modification factor and forward-backward production ratio.
- [56] LHCb collaboration, R. Aaij *et al.*, *Measurement of the track reconstruction efficiency at LHCb*, JINST **10** (2015) P02007, [arXiv:1408.1251](#).
- [57] L. Anderlini *et al.*, *The PIDCalib package*, LHCb-PUB-2016-021, 2016.
- [58] R. Aaij *et al.*, *Selection and processing of calibration samples to measure the particle identification performance of the LHCb experiment in Run 2*, Eur. Phys. J. Tech. Instr. **6** (2019) 1, [arXiv:1803.00824](#).
- [59] LHCb collaboration, R. Aaij *et al.*, *Measurements of prompt charm production cross-sections in pp collisions at $\sqrt{s} = 5 \text{ TeV}$* , JHEP **06** (2017) 147, [arXiv:1610.02230](#).
- [60] LHCb collaboration, R. Aaij *et al.*, *Measurements of prompt charm production cross-sections in pp collisions at $\sqrt{s} = 13 \text{ TeV}$* , JHEP **03** (2016) 159, Erratum *ibid.* **09** (2016) 013, Erratum *ibid.* **05** (2017) 074, [arXiv:1510.01707](#).
- [61] A. Kusina, J.-P. Lansberg, I. Schienbein, and H.-S. Shao, *Gluon shadowing in heavy-flavor production at the lhc*, Phys. Rev. Lett. **121** (2018) 052004.
- [62] H.-S. Shao, *HELAC-Onia: An automatic matrix element generator for heavy quarkonium physics*, Comput. Phys. Commun. **184** (2013) 2562, [arXiv:1212.5293](#).
- [63] H.-S. Shao, *HELAC-Onia 2.0: an upgraded matrix-element and event generator for heavy quarkonium physics*, Comput. Phys. Commun. **198** (2016) 238, [arXiv:1507.03435](#).
- [64] K. J. Eskola, P. Paakkinen, H. Paukkunen, and C. A. Salgado, *EPPS16: Nuclear parton distributions with LHC data*, Eur. Phys. J. **C77** (2017) 163, [arXiv:1612.05741](#).
- [65] K. Kovarik *et al.*, *nCTEQ15 - Global analysis of nuclear parton distributions with uncertainties in the CTEQ framework*, Phys. Rev. **D93** (2016) 085037, [arXiv:1509.00792](#).
- [66] J.-P. Lansberg and H.-S. Shao, *Towards an automated tool to evaluate the impact of the nuclear modification of the gluon density on quarkonium, D and B meson production in proton–nucleus collisions*, Eur. Phys. J. **C77** (2017) 1, [arXiv:1610.05382](#).
- [67] B. Ducloué, T. Lappi, and H. Mäntysaari, *Forward J/ψ production in proton-nucleus collisions at high energy*, Phys. Rev. **D91** (2015) 114005, [arXiv:1503.02789](#).
- [68] B. Ducloué, T. Lappi, and H. Mäntysaari, *Forward J/ψ and D meson nuclear suppression at the LHC*, Nucl. Part. Phys. Proc. **289-290** (2017) 309, [arXiv:1612.04585](#).
- [69] Y.-Q. Ma, P. Tribedy, R. Venugopalan, and K. Watanabe, *Event engineering studies for heavy flavor production and hadronization in high multiplicity hadron-hadron and hadron-nucleus collisions*, Phys. Rev. **D98** (2018) 074025, [arXiv:1803.11093](#).
- [70] H. Kowalski, T. Lappi, and R. Venugopalan, *Nuclear enhancement of universal dynamics of high parton densities*, Phys. Rev. Lett. **100** (2008) 022303 [arXiv:0705.3047](#).

LHCb collaboration

R. Aaij³² , A.S.W. Abdelmotteleb⁵⁰ , C. Abellan Beteta⁴⁴, F. Abudinén⁵⁰ , T. Ackernley⁵⁴ , B. Adeva⁴⁰ , M. Adinolfi⁴⁸ , H. Afsharnia⁹, C. Agapopoulou¹³ , C.A. Aidala⁷⁶ , S. Aiola²⁵ , Z. Ajaltouni⁹, S. Akar⁵⁹ , K. Akiba³² , J. Albrecht¹⁵ , F. Alessio⁴² , M. Alexander⁵³ , A. Alfonso Albero³⁹ , Z. Aliouche⁵⁶ , P. Alvarez Cartelle⁴⁹ , S. Amato² , J.L. Amey⁴⁸ , Y. Amhis^{11,42} , L. An⁴² , L. Anderlini²² , M. Andersson⁴⁴ , A. Andreianov³⁸ , M. Andreotti²¹ , D. Andreou⁶² , D. Ao⁶ , F. Archilli¹⁷ , A. Artamonov³⁸ , M. Artuso⁶² , E. Aslanides¹⁰ , M. Atzeni⁴⁴ , B. Audurier¹² , S. Bachmann¹⁷ , M. Bachmayer⁴³ , J.J. Back⁵⁰ , A. Bailly-reyre¹³, P. Baladron Rodriguez⁴⁰ , V. Balagura¹² , W. Baldini²¹ , J. Baptista de Souza Leite¹ , M. Barbetti^{22,j} , R.J. Barlow⁵⁶ , S. Barsuk¹¹ , W. Barter⁵⁵ , M. Bartolini⁴⁹ , F. Baryshnikov³⁸ , J.M. Basels¹⁴ , G. Bassi^{29,q} , B. Batsukh⁴ , A. Battig¹⁵ , A. Bay⁴³ , A. Beck⁵⁰ , M. Becker¹⁵ , F. Bedeschi²⁹ , I.B. Bediaga¹ , A. Beiter⁶², V. Belavin³⁸, S. Belin⁴⁰ , V. Bellee⁴⁴ , K. Belous³⁸ , I. Belov³⁸ , I. Belyaev³⁸ , G. Bencivenni²³ , E. Ben-Haim¹³ , A. Berezhnoy³⁸ , R. Bernet⁴⁴ , D. Berninghoff¹⁷, H.C. Bernstein⁶², C. Bertella⁵⁶ , A. Bertolin²⁸ , C. Betancourt⁴⁴ , F. Betti⁴² , Ia. Bezshyiko⁴⁴ , S. Bhasin⁴⁸ , J. Bhom³⁵ , L. Bian⁶⁷ , M.S. Bieker¹⁵ , N.V. Biesuz²¹ , S. Bifani⁴⁷ , P. Billoir¹³ , A. Biolchini³² , M. Birch⁵⁵ , F.C.R. Bishop⁴⁹ , A. Bitadze⁵⁶ , A. Bizzeti , M.P. Blago⁴⁹ , T. Blake⁵⁰ , F. Blanc⁴³ , S. Blusk⁶² , D. Bobulska⁵³ , J.A. Boelhauve¹⁵ , O. Boente Garcia⁴⁰ , T. Boettcher⁵⁹ , A. Boldyrev³⁸ , N. Bondar^{38,42} , S. Borghi⁵⁶ , M. Borsato¹⁷ , J.T. Borsuk³⁵ , S.A. Bouchiba⁴³ , T.J.V. Bowcock^{54,42} , A. Boyer⁴² , C. Bozzi²¹ , M.J. Bradley⁵⁵, S. Braun⁶⁰ , A. Brea Rodriguez⁴⁰ , J. Brodzicka³⁵ , A. Brossa Gonzalo⁵⁰ , D. Brundu²⁷ , A. Buonaura⁴⁴ , L. Buonincontri²⁸ , A.T. Burke⁵⁶ , C. Burr⁴² , A. Bursche⁶⁶, A. Butkevich³⁸ , J.S. Butter³² , J. Buytaert⁴² , W. Byczynski⁴² , S. Cadeddu²⁷ , H. Cai⁶⁷, R. Calabrese^{21,i} , L. Calefice^{15,13} , S. Cali²³ , R. Calladine⁴⁷, M. Calvi^{26,m} , M. Calvo Gomez⁷⁴ , P. Camargo Magalhaes⁴⁸ , P. Campana²³ , D.H. Campora Perez⁷³ , A.F. Campoverde Quezada⁶ , S. Capelli^{26,m} , L. Capriotti^{20,g} , A. Carbone^{20,g} , G. Carboni³¹ , R. Cardinale^{24,k} , A. Cardini²⁷ , I. Carli⁴ , P. Carniti^{26,m} , L. Carus¹⁴, A. Casais Vidal⁴⁰ , R. Caspary¹⁷ , G. Casse⁵⁴ , M. Cattaneo⁴² , G. Cavallero⁴² , V. Cavallini^{21,i} , S. Celani⁴³ , J. Cerasoli¹⁰ , D. Cervenkov⁵⁷ , A.J. Chadwick⁵⁴ , M.G. Chapman⁴⁸, M. Charles¹³ , Ph. Charpentier⁴² , C.A. Chavez Barajas⁵⁴ , M. Chefdeville⁸ , C. Chen³ , S. Chen⁴ , A. Chernov³⁵ , S. Chernyshenko⁴⁶ , V. Chobanova⁴⁰ , S. Cholak⁴³ , M. Chrzaszcz³⁵ , A. Chubykin³⁸ , V. Chulikov³⁸ , P. Ciambrone²³ , M.F. Cicala⁵⁰ , X. Cid Vidal⁴⁰ , G. Ciezarek⁴² , G. Ciullo^{i,21} , P.E.L. Clarke⁵² , M. Clemencic⁴² , H.V. Cliff⁴⁹ , J. Closier⁴² , J.L. Cobbledick⁵⁶ , V. Coco⁴² , J.A.B. Coelho¹¹ , J. Cogan¹⁰ , E. Cogneras⁹ , L. Cojocariu³⁷ , P. Collins⁴² , T. Colombo⁴² , L. Congedo¹⁹ , A. Contu²⁷ , N. Cooke⁴⁷ , G. Coombs⁵³ , I. Corredoira⁴⁰ , G. Corti⁴² , B. Couturier⁴² , D.C. Craik⁵⁸ , J. Crkovská⁶¹ , M. Cruz Torres^{1,e} , R. Currie⁵² , C.L. Da Silva⁶¹ , S. Dadabaev³⁸ , L. Dai⁶⁵ , E. Dall'Occo¹⁵ , J. Dalseno⁴⁰ , C. D'Ambrosio⁴² , A. Danilina³⁸ , P. d'Argent¹⁵ , J.E. Davies⁵⁶ , A. Davis⁵⁶ , O. De Aguiar Francisco⁵⁶ , J. de Boer⁴² , K. De Bruyn⁷² , S. De Capua⁵⁶ , M. De Cian⁴³ , U. De Freitas Carneiro Da Graca¹ , E. De Lucia²³ , J.M. De Miranda¹ , L. De Paula² , M. De Serio^{19,f} , D. De Simone⁴⁴ , P. De Simone²³ , F. De Vellis¹⁵ , J.A. de Vries⁷³ , C.T. Dean⁶¹ , F. Debernardis^{19,f} , D. Decamp⁸ , V. Dedu¹⁰ , L. Del Buono¹³ , B. Delaney⁵⁸ , H.-P. Dembinski¹⁵ , V. Denysenko⁴⁴ , O. Deschamps⁹ , F. Dettori^{27,h} , B. Dey⁷⁰ , A. Di Cicco²³ , P. Di Nezza²³ , S. Didenko³⁸ , L. Dieste Maronas⁴⁰, S. Ding⁶² , V. Dobishuk⁴⁶ , A. Dolmatov³⁸, C. Dong³ 

A.M. Donohoe¹⁸ [ID](#), F. Dordei²⁷ [ID](#), A.C. dos Reis¹ [ID](#), L. Douglas⁵³, A.G. Downes⁸ [ID](#),
 M.W. Dudek³⁵ [ID](#), L. Dufour⁴² [ID](#), V. Duk⁷¹ [ID](#), P. Durante⁴² [ID](#), J.M. Durham⁶¹ [ID](#),
 D. Dutta⁵⁶ [ID](#), A. Dziurda³⁵ [ID](#), A. Dzyuba³⁸ [ID](#), S. Easo⁵¹ [ID](#), U. Egede⁶³ [ID](#), V. Egorychev³⁸ [ID](#),
 S. Eidelman^{38,†}, S. Eisenhardt⁵² [ID](#), S. Ek-In⁴³ [ID](#), L. Eklund⁷⁵ [ID](#), S. Ely⁶² [ID](#), A. Ene³⁷ [ID](#),
 E. Epple⁶¹ [ID](#), S. Escher¹⁴ [ID](#), J. Eschle⁴⁴ [ID](#), S. Esen⁴⁴ [ID](#), T. Evans⁵⁶ [ID](#), L.N. Falcao¹ [ID](#),
 Y. Fan⁶ [ID](#), B. Fang⁶⁷ [ID](#), S. Farry⁵⁴ [ID](#), D. Fazzini^{26,m} [ID](#), M. Feo⁴² [ID](#), A.D. Fernez⁶⁰ [ID](#),
 F. Ferrari²⁰ [ID](#), L. Ferreira Lopes⁴³ [ID](#), F. Ferreira Rodrigues² [ID](#), S. Ferreres Sole³² [ID](#),
 M. Ferrillo⁴⁴ [ID](#), M. Ferro-Luzzi⁴² [ID](#), S. Filippov³⁸ [ID](#), R.A. Fini¹⁹ [ID](#), M. Fiorini^{21,i} [ID](#),
 M. Firlej³⁴ [ID](#), K.M. Fischer⁵⁷ [ID](#), D.S. Fitzgerald⁷⁶ [ID](#), C. Fitzpatrick⁵⁶ [ID](#), T. Fiutowski³⁴ [ID](#),
 F. Fleuret¹² [ID](#), M. Fontana¹³ [ID](#), F. Fontanelli^{24,k} [ID](#), R. Forty⁴² [ID](#), D. Foulds-Holt⁴⁹ [ID](#),
 V. Franco Lima⁵⁴ [ID](#), M. Franco Sevilla⁶⁰ [ID](#), M. Frank⁴² [ID](#), E. Franzoso^{21,i} [ID](#), G. Frau¹⁷ [ID](#),
 C. Frei⁴² [ID](#), D.A. Friday⁵³ [ID](#), J. Fu⁶ [ID](#), Q. Fuehring¹⁵ [ID](#), E. Gabriel³² [ID](#), G. Galati^{19,f} [ID](#),
 A. Gallas Torreira⁴⁰ [ID](#), D. Galli^{20,g} [ID](#), S. Gambetta^{52,42} [ID](#), Y. Gan³ [ID](#), M. Gandelman² [ID](#),
 P. Gandini²⁵ [ID](#), Y. Gao⁵ [ID](#), M. Garau^{27,h} [ID](#), L.M. Garcia Martin⁵⁰ [ID](#), P. Garcia Moreno³⁹ [ID](#),
 J. García Pardiñas^{26,m} [ID](#), B. Garcia Plana⁴⁰, F.A. Garcia Rosales¹² [ID](#), L. Garrido³⁹ [ID](#),
 C. Gaspar⁴² [ID](#), R.E. Geertsema³² [ID](#), D. Gerick¹⁷, L.L. Gerken¹⁵ [ID](#), E. Gersabeck⁵⁶ [ID](#),
 M. Gersabeck⁵⁶ [ID](#), T. Gershon⁵⁰ [ID](#), L. Giambastiani²⁸ [ID](#), V. Gibson⁴⁹ [ID](#), H.K. Giemza³⁶ [ID](#),
 A.L. Gilman⁵⁷ [ID](#), M. Giovannetti^{23,t} [ID](#), A. Gioventù⁴⁰ [ID](#), P. Gironella Gironell³⁹ [ID](#),
 C. Giugliano^{21,i} [ID](#), M.A. Giza³⁵ [ID](#), K. Gizdov⁵² [ID](#), E.L. Gkougkousis⁴² [ID](#), V.V. Gligorov^{13,42} [ID](#),
 C. Göbel⁶⁴ [ID](#), E. Golobardes⁷⁴ [ID](#), D. Golubkov³⁸ [ID](#), A. Golutvin^{55,38} [ID](#), A. Gomes^{1,a} [ID](#),
 S. Gomez Fernandez³⁹ [ID](#), F. Goncalves Abrantes⁵⁷ [ID](#), M. Goncerz³⁵ [ID](#), G. Gong³ [ID](#),
 I.V. Gorelov³⁸ [ID](#), C. Gotti²⁶ [ID](#), J.P. Grabowski¹⁷ [ID](#), T. Grammatico¹³ [ID](#),
 L.A. Granado Cardoso⁴² [ID](#), E. Grauges³⁹ [ID](#), E. Graverini⁴³ [ID](#), G. Graziani [ID](#), A. T. Grecu³⁷ [ID](#),
 L.M. Greeven³² [ID](#), N.A. Grieser⁴ [ID](#), L. Grillo⁵³ [ID](#), S. Gromov³⁸ [ID](#), B.R. Gruberg Cazon⁵⁷ [ID](#), C.
 Gu³ [ID](#), M. Guarise^{21,i} [ID](#), M. Guittiere¹¹ [ID](#), P. A. Günther¹⁷ [ID](#), E. Gushchin³⁸ [ID](#), A. Guth¹⁴,
 Y. Guz³⁸ [ID](#), T. Gys⁴² [ID](#), T. Hadavizadeh⁶³ [ID](#), G. Haefeli⁴³ [ID](#), C. Haen⁴² [ID](#), J. Haimberger⁴² [ID](#),
 S.C. Haines⁴⁹ [ID](#), T. Halewood-leagas⁵⁴ [ID](#), M.M. Halvorsen⁴² [ID](#), P.M. Hamilton⁶⁰ [ID](#),
 J. Hammerich⁵⁴ [ID](#), Q. Han⁷ [ID](#), X. Han¹⁷ [ID](#), E.B. Hansen⁵⁶ [ID](#), S. Hansmann-Menzemer^{17,42} [ID](#),
 L. Hao⁶ [ID](#), N. Harnew⁵⁷ [ID](#), T. Harrison⁵⁴ [ID](#), C. Hasse⁴² [ID](#), M. Hatch⁴² [ID](#), J. He^{6,c} [ID](#),
 K. Heijhoff³² [ID](#), K. Heinicke¹⁵ [ID](#), R.D.L. Henderson^{63,50} [ID](#), A.M. Hennequin⁵⁸ [ID](#),
 K. Hennessy⁵⁴ [ID](#), L. Henry⁴² [ID](#), J. Heuel¹⁴ [ID](#), A. Hicheur² [ID](#), D. Hill⁴³ [ID](#), M. Hilton⁵⁶ [ID](#),
 S.E. Hollitt¹⁵ [ID](#), R. Hou⁷ [ID](#), Y. Hou⁸ [ID](#), J. Hu¹⁷, J. Hu⁶⁶ [ID](#), W. Hu⁵ [ID](#), X. Hu³ [ID](#),
 W. Huang⁶ [ID](#), X. Huang⁶⁷, W. Hulsbergen³² [ID](#), R.J. Hunter⁵⁰ [ID](#), M. Hushchyn³⁸ [ID](#),
 D. Hutchcroft⁵⁴ [ID](#), P. Ibis¹⁵ [ID](#), M. Idzik³⁴ [ID](#), D. Ilin³⁸ [ID](#), P. Ilten⁵⁹ [ID](#), A. Inglessi³⁸ [ID](#),
 A. Iniukhin³⁸ [ID](#), A. Ishteev³⁸ [ID](#), K. Ivshin³⁸ [ID](#), R. Jacobsson⁴² [ID](#), H. Jage¹⁴ [ID](#),
 S.J. Jaimes Elles⁴¹ [ID](#), S. Jakobsen⁴² [ID](#), E. Jans³² [ID](#), B.K. Jashal⁴¹ [ID](#), A. Jawahery⁶⁰ [ID](#),
 V. Jevtic¹⁵ [ID](#), X. Jiang^{4,6} [ID](#), M. John⁵⁷ [ID](#), D. Johnson⁵⁸ [ID](#), C.R. Jones⁴⁹ [ID](#), T.P. Jones⁵⁰ [ID](#),
 B. Jost⁴² [ID](#), N. Jurik⁴² [ID](#), I. Juszczak³⁵ [ID](#), S. Kandybei⁴⁵ [ID](#), Y. Kang³ [ID](#), M. Karacson⁴² [ID](#),
 D. Karpenkov³⁸ [ID](#), M. Karpov³⁸ [ID](#), J.W. Kautz⁵⁹ [ID](#), F. Keizer⁴² [ID](#), D.M. Keller⁶² [ID](#),
 M. Kenzie⁵⁰ [ID](#), T. Ketel³³ [ID](#), B. Khanji¹⁵ [ID](#), A. Kharisova³⁸ [ID](#), S. Kholodenko³⁸ [ID](#),
 T. Kirn¹⁴ [ID](#), V.S. Kirsebom⁴³ [ID](#), O. Kitouni⁵⁸ [ID](#), S. Klaver³³ [ID](#), N. Kleijne^{29,q} [ID](#),
 K. Klimaszewski³⁶ [ID](#), M.R. Kmiec³⁶ [ID](#), S. Kolliiev⁴⁶ [ID](#), A. Kondybayaeva³⁸ [ID](#),
 A. Konoplyannikov³⁸ [ID](#), P. Kopciewicz³⁴ [ID](#), R. Kopecna¹⁷, P. Koppenburg³² [ID](#),
 M. Korolev³⁸ [ID](#), I. Kostiuk^{32,46} [ID](#), O. Kot⁴⁶, S. Kotriakhova [ID](#), A. Kozachuk³⁸ [ID](#),
 P. Kravchenko³⁸ [ID](#), L. Kravchuk³⁸ [ID](#), R.D. Krawczyk⁴² [ID](#), M. Kreps⁵⁰ [ID](#), S. Kretzschmar¹⁴ [ID](#),
 P. Krokovny³⁸ [ID](#), W. Krupa³⁴ [ID](#), W. Krzemien³⁶ [ID](#), J. Kubat¹⁷, W. Kucewicz^{35,34} [ID](#),
 M. Kucharczyk³⁵ [ID](#), V. Kudryavtsev³⁸ [ID](#), G.J. Kunde⁶¹, D. Lacarrere⁴² [ID](#), G. Lafferty⁵⁶ [ID](#),
 A. Lai²⁷ [ID](#), A. Lampis^{27,h} [ID](#), D. Lancierini⁴⁴ [ID](#), J.J. Lane⁵⁶ [ID](#), R. Lane⁴⁸ [ID](#), G. Lanfranchi²³ [ID](#),
 C. Langenbruch¹⁴ [ID](#), J. Langer¹⁵ [ID](#), O. Lantwin³⁸ [ID](#), T. Latham⁵⁰ [ID](#), F. Lazzari^{29,u} [ID](#),
 M. Lazzaroni^{25,l} [ID](#), R. Le Gac¹⁰ [ID](#), S.H. Lee⁷⁶ [ID](#), R. Lefèvre⁹ [ID](#), A. Leflat³⁸ [ID](#), S. Legotin³⁸ [ID](#)

- P. Lenisa^{i,21} , O. Leroy¹⁰ , T. Lesiak³⁵ , B. Leverington¹⁷ , H. Li⁶⁶ , K. Li⁷ ,
P. Li¹⁷ , S. Li⁷ , Y. Li⁴ , Z. Li⁶² , X. Liang⁶² , C. Lin⁶ , T. Lin⁵¹ , R. Lindner⁴² ,
V. Lisovskyi¹⁵ , R. Litvinov^{27,h} , G. Liu⁶⁶ , H. Liu⁶ , Q. Liu⁶ , S. Liu^{4,6} ,
A. Lobo Salvia³⁹ , A. Loi²⁷ , R. Lollini⁷¹ , J. Lomba Castro⁴⁰ , I. Longstaff⁵³ ,
J.H. Lopes² , S. López Soliño⁴⁰ , G.H. Lovell⁴⁹ , Y. Lu^{4,b} , C. Lucarelli^{22,j} ,
D. Lucchesi^{28,o} , S. Luchuk³⁸ , M. Lucio Martinez³² , V. Lukashenko^{32,46} , Y. Luo³ ,
A. Lupato⁵⁶ , E. Luppi^{21,i} , A. Lusiani^{29,q} , K. Lynch¹⁸ , X.-R. Lyu⁶ , L. Ma⁴ ,
R. Ma⁶ , S. Maccolini²⁰ , F. Machefert¹¹ , F. Maciuc³⁷ , V. Macko⁴³ ,
P. Mackowiak¹⁵ , S. Maddrell-Mander⁴⁸ , L.R. Madhan Mohan⁴⁸ , A. Maevskiy³⁸ ,
D. Maisuzenko³⁸ , M.W. Majewski³⁴ , J.J. Malczewski³⁵ , S. Malde⁵⁷ , B. Malecki³⁵ ,
A. Malinin³⁸ , T. Maltsev³⁸ , H. Malygina¹⁷ , G. Manca^{27,h} , G. Mancinelli¹⁰ ,
D. Manuzzi²⁰ , C.A. Manzari⁴⁴ , D. Marangotto^{25,l} , J.F. Marchand⁸ , U. Marconi²⁰ ,
S. Mariani^{22,j} , C. Marin Benito³⁹ , M. Marinangeli⁴³ , J. Marks¹⁷ , A.M. Marshall⁴⁸ ,
P.J. Marshall⁵⁴ , G. Martelli^{71,p} , G. Martellotti³⁰ , L. Martinazzoli^{42,m} ,
M. Martinelli^{26,m} , D. Martinez Santos⁴⁰ , F. Martinez Vidal⁴¹ , A. Massafferri¹ ,
M. Materok¹⁴ , R. Matev⁴² , A. Mathad⁴⁴ , V. Matiunin³⁸ , C. Matteuzzi²⁶ ,
K.R. Mattioli⁷⁶ , A. Mauri³² , E. Maurice¹² , J. Mauricio³⁹ , M. Mazurek⁴² ,
M. McCann⁵⁵ , L. Mcconnell¹⁸ , T.H. McGrath⁵⁶ , N.T. McHugh⁵³ , A. McNab⁵⁶ ,
R. McNulty¹⁸ , J.V. Mead⁵⁴ , B. Meadows⁵⁹ , G. Meier¹⁵ , D. Melnychuk³⁶ ,
S. Meloni^{26,m} , M. Merk^{32,73} , A. Merli^{25,l} , L. Meyer Garcia² , M. Mikhasenko^{69,d} ,
D.A. Milanes⁶⁸ , E. Millard⁵⁰ , M. Milovanovic⁴² , M.-N. Minard^{8,\dagger} , A. Minotti^{26,m} ,
S.E. Mitchell⁵² , B. Mitreska⁵⁶ , D.S. Mitzel¹⁵ , A. Mödden¹⁵ , R.A. Mohammed⁵⁷ ,
R.D. Moise⁵⁵ , S. Mokhnenco³⁸ , T. Mombächer⁴⁰ , I.A. Monroy⁶⁸ , S. Monteil⁹ ,
M. Morandin²⁸ , G. Morello²³ , M.J. Morello^{29,q} , J. Moron³⁴ , A.B. Morris⁶⁹ ,
A.G. Morris⁵⁰ , R. Mountain⁶² , H. Mu³ , F. Muheim⁵² , M. Mulder⁷² , K. Müller⁴⁴ ,
C.H. Murphy⁵⁷ , D. Murray⁵⁶ , R. Murta⁵⁵ , P. Muzzetto^{27,h} , P. Naik⁴⁸ ,
T. Nakada⁴³ , R. Nandakumar⁵¹ , T. Nanut⁴² , I. Nasteva² , M. Needham⁵² ,
N. Neri^{25,l} , S. Neubert⁶⁹ , N. Neufeld⁴² , P. Neustroev³⁸ , R. Newcombe⁵⁵ , E.M. Niel⁴³ ,
S. Nieswand¹⁴ , N. Nikitin³⁸ , N.S. Nolte⁵⁸ , C. Normand^{8,h,27} , C. Nunez⁷⁶ ,
A. Oblakowska-Mucha³⁴ , V. Obraztsov³⁸ , T. Oeser¹⁴ , D.P. O'Hanlon⁴⁸ ,
S. Okamura^{21,i} , R. Oldeman^{27,h} , F. Oliva⁵² , M.E. Olivares⁶² , C.J.G. Onderwater⁷² ,
R.H. O'Neil⁵² , J.M. Otalora Goicochea² , T. Ovsiannikova³⁸ , P. Owen⁴⁴ ,
A. Oyanguren⁴¹ , O. Ozcelik⁵² , K.O. Padeken⁶⁹ , B. Pagare⁵⁰ , P.R. Pais⁴² ,
T. Pajero⁵⁷ , A. Palano¹⁹ , M. Palutan²³ , Y. Pan⁵⁶ , G. Panshin³⁸ ,
A. Papanestis⁵¹ , M. Pappagallo^{19,f} , L.L. Pappalardo^{21,i} , C. Pappenheimer⁵⁹ ,
W. Parker⁶⁰ , C. Parkes⁵⁶ , B. Passalacqua^{21,i} , G. Passaleva²² , A. Pastore¹⁹ ,
M. Patel⁵⁵ , C. Patrignani^{20,g} , C.J. Pawley⁷³ , A. Pearce⁴² , A. Pellegrino³² ,
M. Pepe Altarelli⁴² , S. Perazzini²⁰ , D. Pereima Castro⁴⁰ , P. Perret⁹ ,
M. Petric⁵³ , K. Petridis⁴⁸ , A. Petrolini^{24,k} , A. Petrov³⁸ , S. Petrucci⁵² , M. Petruzzo²⁵ ,
H. Pham⁶² , A. Philippov³⁸ , R. Piandani⁶ , L. Pica^{29,q} , M. Piccini⁷¹ , B. Pietrzyk⁸ ,
G. Pietrzyk¹¹ , M. Pili⁵⁷ , D. Pinci³⁰ , F. Pisani⁴² , M. Pizzichemi^{26,m,42} ,
V. Placinta³⁷ , J. Plews⁴⁷ , M. Plo Casasus⁴⁰ , F. Polci^{13,42} , M. Poli Lener²³ ,
M. Poliakova⁶² , A. Poluektov¹⁰ , N. Polukhina³⁸ , I. Polyakov⁶² , E. Polycarpo² ,
S. Ponce⁴² , D. Popov^{6,42} , S. Popov³⁸ , S. Poslavskii³⁸ , K. Prasant³⁵ ,
L. Promberger⁴² , C. Prouve⁴⁰ , V. Pugatch⁴⁶ , V. Puill¹¹ , G. Punzi^{29,r} , H.R. Qi³ ,
W. Qian⁶ , N. Qin³ , S. Qu³ , R. Quagliani⁴³ , N.V. Raab¹⁸ , R.I. Rabadan Trejo⁶ ,
B. Rachwal³⁴ , J.H. Rademacker⁴⁸ , R. Rajagopalan⁶² , M. Rama²⁹ ,
M. Ramos Pernas⁵⁰ , M.S. Rangel² , F. Ratnikov³⁸ , G. Raven^{33,42} ,
M. Rebollo De Miguel⁴¹ , F. Redi⁴² , F. Reiss⁵⁶ , C. Remon Alepuz⁴¹ , Z. Ren³ ,
V. Renaudin⁵⁷ , P.K. Resmi¹⁰ , R. Ribatti^{29,q} , A.M. Ricci²⁷ , S. Ricciardi⁵¹ ,

- K. Rinnert⁵⁴ , P. Robbe¹¹ , G. Robertson⁵² , A.B. Rodrigues⁴³ , E. Rodrigues⁵⁴ , J.A. Rodriguez Lopez⁶⁸ , E. Rodriguez Rodriguez⁴⁰ , A. Rollings⁵⁷ , P. Roloff⁴² , V. Romanovskiy³⁸ , M. Romero Lamas⁴⁰ , A. Romero Vidal⁴⁰ , J.D. Roth^{76,†}, M. Rotondo²³ , M.S. Rudolph⁶² , T. Ruf⁴² , R.A. Ruiz Fernandez⁴⁰ , J. Ruiz Vidal⁴¹, A. Ryzhikov³⁸ , J. Ryzka³⁴ , J.J. Saborido Silva⁴⁰ , N. Sagidova³⁸ , N. Sahoo⁴⁷ , B. Saitta^{27,h} , M. Salomoni⁴² , C. Sanchez Gras³² , I. Sanderswood⁴¹ , R. Santacesaria³⁰ , C. Santamarina Rios⁴⁰ , M. Santimaria²³ , E. Santovetti^{31,t} , D. Saranin³⁸ , G. Sarpis¹⁴ , M. Sarpis⁶⁹ , A. Sarti³⁰ , C. Satriano^{30,s} , A. Satta³¹ , M. Saur¹⁵ , D. Savrina³⁸ , H. Sazak⁹ , L.G. Scantlebury Smead⁵⁷ , A. Scarabotto¹³ , S. Schael¹⁴ , S. Scherl⁵⁴ , M. Schiller⁵³ , H. Schindler⁴² , M. Schmelling¹⁶ , B. Schmidt⁴² , S. Schmitt¹⁴ , O. Schneider⁴³ , A. Schopper⁴² , M. Schubiger³² , S. Schulte⁴³ , M.H. Schune¹¹ , R. Schwemmer⁴² , B. Sciascia^{23,42} , A. Sciuccati⁴² , S. Sellam⁴⁰ , A. Semennikov³⁸ , M. Senghi Soares³³ , A. Sergi^{24,k} , N. Serra⁴⁴ , L. Sestini²⁸ , A. Seuthe¹⁵ , Y. Shang⁵ , D.M. Shangase⁷⁶ , M. Shapkin³⁸ , I. Shchemerov³⁸ , L. Shchutska⁴³ , T. Shears⁵⁴ , L. Shekhtman³⁸ , Z. Shen⁵ , S. Sheng^{4,6} , V. Shevchenko³⁸ , E.B. Shields^{26,m} , Y. Shimizu¹¹ , E. Shmanin³⁸ , J.D. Shupperd⁶² , B.G. Siddi^{21,i} , R. Silva Coutinho⁴⁴ , G. Simi²⁸ , S. Simone^{19,f} , M. Singla⁶³ , N. Skidmore⁵⁶ , R. Skuza¹⁷ , T. Skwarnicki⁶² , M.W. Slater⁴⁷ , I. Slazyk^{21,i} , J.C. Smallwood⁵⁷ , J.G. Smeaton⁴⁹ , E. Smith⁴⁴ , M. Smith⁵⁵ , A. Snoch³² , L. Soares Lavra⁹ , M.D. Sokoloff⁵⁹ , F.J.P. Soler⁵³ , A. Solomin^{38,48} , A. Solovev³⁸ , I. Solovyev³⁸ , F.L. Souza De Almeida² , B. Souza De Paula² , B. Spaan^{15,†}, E. Spadaro Norella^{25,l} , E. Spiridenkov³⁸ , P. Spradlin⁵³ , V. Sriskaran⁴² , F. Stagni⁴² , M. Stahl⁵⁹ , S. Stahl⁴² , S. Stanislaus⁵⁷ , O. Steinkamp⁴⁴ , O. Stenyakin³⁸ , H. Stevens¹⁵ , S. Stone^{62,†} , D. Strekalina³⁸ , F. Suljik⁵⁷ , J. Sun²⁷ , L. Sun⁶⁷ , Y. Sun⁶⁰ , P. Svihra⁵⁶ , P.N. Swallow⁴⁷ , K. Swientek³⁴ , A. Szabelski³⁶ , T. Szumlak³⁴ , M. Szymanski⁴² , S. Taneja⁵⁶ , A.R. Tanner⁴⁸ , M.D. Tat⁵⁷ , A. Terentev³⁸ , F. Teubert⁴² , E. Thomas⁴² , D.J.D. Thompson⁴⁷ , K.A. Thomson⁵⁴ , H. Tilquin⁵⁵ , V. Tisserand⁹ , S. T'Jampens⁸ , M. Tobin⁴ , L. Tomassetti^{21,i} , G. Tonani^{25,l} , X. Tong⁵ , D. Torres Machado¹ , D.Y. Tou³ , E. Trifonova³⁸ , S.M. Trilov⁴⁸ , C. Tripli⁴³ , G. Tuci⁶ , A. Tully⁴³ , N. Tuning^{32,42} , A. Ukleja³⁶ , D.J. Unverzagt¹⁷ , E. Ursov³⁸ , A. Usachov³² , A. Ustyuzhanin³⁸ , U. Uwer¹⁷ , A. Vagner³⁸ , V. Vagnoni²⁰ , A. Valassi⁴² , G. Valenti²⁰ , N. Valls Canudas⁷⁴ , M. van Beuzekom³² , M. Van Dijk⁴³ , H. Van Hecke⁶¹ , E. van Herwijnen³⁸ , M. van Veghel⁷² , R. Vazquez Gomez³⁹ , P. Vazquez Regueiro⁴⁰ , C. Vázquez Sierra⁴² , S. Vecchi²¹ , J.J. Velthuis⁴⁸ , M. Veltri^{22,v} , A. Venkateswaran⁶² , M. Veronesi³² , M. Vesterinen⁵⁰ , D. Vieira⁵⁹ , M. Vieites Diaz⁴³ , X. Vilasis-Cardona⁷⁴ , E. Vilella Figueras⁵⁴ , A. Villa²⁰ , P. Vincent¹³ , F.C. Volle¹¹ , D. vom Bruch¹⁰ , A. Vorobyev³⁸ , V. Vorobyev³⁸ , N. Voropaev³⁸ , K. Vos⁷³ , R. Waldi¹⁷ , J. Walsh²⁹ , C. Wang¹⁷ , J. Wang⁵ , J. Wang⁴ , J. Wang³ , J. Wang⁶⁷ , M. Wang⁵ , R. Wang⁴⁸ , Y. Wang⁷ , Z. Wang⁴⁴ , Z. Wang³ , Z. Wang⁶ , J.A. Ward^{50,63} , N.K. Watson⁴⁷ , D. Websdale⁵⁵ , C. Weisser⁵⁸ , B.D.C. Westhenry⁴⁸ , D.J. White⁵⁶ , M. Whitehead⁵³ , A.R. Wiederhold⁵⁰ , D. Wiedner¹⁵ , G. Wilkinson⁵⁷ , M.K. Wilkinson⁵⁹ , I. Williams⁴⁹ , M. Williams⁵⁸ , M.R.J. Williams⁵² , R. Williams⁴⁹ , F.F. Wilson⁵¹ , W. Wislicki³⁶ , M. Witek³⁵ , L. Witola¹⁷ , C.P. Wong⁶¹ , G. Wormser¹¹ , S.A. Wotton⁴⁹ , H. Wu⁶² , K. Wyllie⁴² , Z. Xiang⁶ , D. Xiao⁷ , Y. Xie⁷ , A. Xu⁵ , J. Xu⁶ , L. Xu³ , M. Xu⁵⁰ , Q. Xu⁶ , Z. Xu⁹ , D. Yang³ , S. Yang⁶ , Y. Yang⁶ , Z. Yang⁵ , Z. Yang⁶⁰ , L.E. Yeomans⁵⁴ , H. Yin⁷ , J. Yu⁶⁵ , X. Yuan⁶² , E. Zaffaroni⁴³ , M. Zavertyaev¹⁶ , M. Zdybal³⁵ , O. Zenaiev⁴² , M. Zeng³ , D. Zhang⁷ , L. Zhang³ , S. Zhang⁶⁵ , S. Zhang⁵ , Y. Zhang⁵ <img alt="ORCID iD icon" data-bbox

V. Zhukov^{14,38} , Q. Zou^{4,6} , S. Zucchelli^{20,9} , D. Zuliani²⁸ , G. Zunică⁵⁶ .

¹Centro Brasileiro de Pesquisas Físicas (CBPF), Rio de Janeiro, Brazil

²Universidade Federal do Rio de Janeiro (UFRJ), Rio de Janeiro, Brazil

³Center for High Energy Physics, Tsinghua University, Beijing, China

⁴Institute Of High Energy Physics (IHEP), Beijing, China

⁵School of Physics State Key Laboratory of Nuclear Physics and Technology, Peking University, Beijing, China

⁶University of Chinese Academy of Sciences, Beijing, China

⁷Institute of Particle Physics, Central China Normal University, Wuhan, Hubei, China

⁸Université Savoie Mont Blanc, CNRS, IN2P3-LAPP, Annecy, France

⁹Université Clermont Auvergne, CNRS/IN2P3, LPC, Clermont-Ferrand, France

¹⁰Aix Marseille Univ, CNRS/IN2P3, CPPM, Marseille, France

¹¹Université Paris-Saclay, CNRS/IN2P3, IJCLab, Orsay, France

¹²Laboratoire Leprince-Ringuet, CNRS/IN2P3, Ecole Polytechnique, Institut Polytechnique de Paris, Palaiseau, France

¹³LPNHE, Sorbonne Université, Paris Diderot Sorbonne Paris Cité, CNRS/IN2P3, Paris, France

¹⁴I. Physikalisches Institut, RWTH Aachen University, Aachen, Germany

¹⁵Fakultät Physik, Technische Universität Dortmund, Dortmund, Germany

¹⁶Max-Planck-Institut für Kernphysik (MPIK), Heidelberg, Germany

¹⁷Physikalischs Institut, Ruprecht-Karls-Universität Heidelberg, Heidelberg, Germany

¹⁸School of Physics, University College Dublin, Dublin, Ireland

¹⁹INFN Sezione di Bari, Bari, Italy

²⁰INFN Sezione di Bologna, Bologna, Italy

²¹INFN Sezione di Ferrara, Ferrara, Italy

²²INFN Sezione di Firenze, Firenze, Italy

²³INFN Laboratori Nazionali di Frascati, Frascati, Italy

²⁴INFN Sezione di Genova, Genova, Italy

²⁵INFN Sezione di Milano, Milano, Italy

²⁶INFN Sezione di Milano-Bicocca, Milano, Italy

²⁷INFN Sezione di Cagliari, Monserrato, Italy

²⁸Università degli Studi di Padova, Università e INFN, Padova, Padova, Italy

²⁹INFN Sezione di Pisa, Pisa, Italy

³⁰INFN Sezione di Roma La Sapienza, Roma, Italy

³¹INFN Sezione di Roma Tor Vergata, Roma, Italy

³²Nikhef National Institute for Subatomic Physics, Amsterdam, Netherlands

³³Nikhef National Institute for Subatomic Physics and VU University Amsterdam, Amsterdam, Netherlands

³⁴AGH - University of Science and Technology, Faculty of Physics and Applied Computer Science, Kraków, Poland

³⁵Henryk Niewodniczanski Institute of Nuclear Physics Polish Academy of Sciences, Kraków, Poland

³⁶National Center for Nuclear Research (NCBJ), Warsaw, Poland

³⁷Horia Hulubei National Institute of Physics and Nuclear Engineering, Bucharest-Magurele, Romania

³⁸Affiliated with an institute covered by a cooperation agreement with CERN

³⁹ICCUB, Universitat de Barcelona, Barcelona, Spain

⁴⁰Instituto Galego de Física de Altas Enerxías (IGFAE), Universidade de Santiago de Compostela, Santiago de Compostela, Spain

⁴¹Instituto de Fisica Corpuscular, Centro Mixto Universidad de Valencia - CSIC, Valencia, Spain

⁴²European Organization for Nuclear Research (CERN), Geneva, Switzerland

⁴³Institute of Physics, Ecole Polytechnique Fédérale de Lausanne (EPFL), Lausanne, Switzerland

⁴⁴Physik-Institut, Universität Zürich, Zürich, Switzerland

⁴⁵NSC Kharkiv Institute of Physics and Technology (NSC KIPT), Kharkiv, Ukraine

⁴⁶Institute for Nuclear Research of the National Academy of Sciences (KINR), Kyiv, Ukraine

⁴⁷University of Birmingham, Birmingham, United Kingdom

⁴⁸H.H. Wills Physics Laboratory, University of Bristol, Bristol, United Kingdom

⁴⁹Cavendish Laboratory, University of Cambridge, Cambridge, United Kingdom

⁵⁰Department of Physics, University of Warwick, Coventry, United Kingdom

- ⁵¹STFC Rutherford Appleton Laboratory, Didcot, United Kingdom
⁵²School of Physics and Astronomy, University of Edinburgh, Edinburgh, United Kingdom
⁵³School of Physics and Astronomy, University of Glasgow, Glasgow, United Kingdom
⁵⁴Oliver Lodge Laboratory, University of Liverpool, Liverpool, United Kingdom
⁵⁵Imperial College London, London, United Kingdom
⁵⁶Department of Physics and Astronomy, University of Manchester, Manchester, United Kingdom
⁵⁷Department of Physics, University of Oxford, Oxford, United Kingdom
⁵⁸Massachusetts Institute of Technology, Cambridge, MA, United States
⁵⁹University of Cincinnati, Cincinnati, OH, United States
⁶⁰University of Maryland, College Park, MD, United States
⁶¹Los Alamos National Laboratory (LANL), Los Alamos, NM, United States
⁶²Syracuse University, Syracuse, NY, United States
⁶³School of Physics and Astronomy, Monash University, Melbourne, Australia, associated to ⁵⁰
⁶⁴Pontifícia Universidade Católica do Rio de Janeiro (PUC-Rio), Rio de Janeiro, Brazil, associated to ²
⁶⁵Physics and Micro Electronic College, Hunan University, Changsha City, China, associated to ⁷
⁶⁶Guangdong Provincial Key Laboratory of Nuclear Science, Guangdong-Hong Kong Joint Laboratory of Quantum Matter, Institute of Quantum Matter, South China Normal University, Guangzhou, China, associated to ³
⁶⁷School of Physics and Technology, Wuhan University, Wuhan, China, associated to ³
⁶⁸Departamento de Física, Universidad Nacional de Colombia, Bogota, Colombia, associated to ¹³
⁶⁹Universität Bonn - Helmholtz-Institut für Strahlen und Kernphysik, Bonn, Germany, associated to ¹⁷
⁷⁰Eotvos Lorand University, Budapest, Hungary, associated to ⁴²
⁷¹INFN Sezione di Perugia, Perugia, Italy, associated to ²¹
⁷²Van Swinderen Institute, University of Groningen, Groningen, Netherlands, associated to ³²
⁷³Universiteit Maastricht, Maastricht, Netherlands, associated to ³²
⁷⁴DS4DS, La Salle, Universitat Ramon Llull, Barcelona, Spain, associated to ³⁹
⁷⁵Department of Physics and Astronomy, Uppsala University, Uppsala, Sweden, associated to ⁵³
⁷⁶University of Michigan, Ann Arbor, MI, United States, associated to ⁶²
- ^aUniversidade Federal do Triângulo Mineiro (UFTM), Uberaba-MG, Brazil
^bCentral South U., Changsha, China
^cHangzhou Institute for Advanced Study, UCAS, Hangzhou, China
^dExcellence Cluster ORIGINS, Munich, Germany
^eUniversidad Nacional Autónoma de Honduras, Tegucigalpa, Honduras
^fUniversità di Bari, Bari, Italy
^gUniversità di Bologna, Bologna, Italy
^hUniversità di Cagliari, Cagliari, Italy
ⁱUniversità di Ferrara, Ferrara, Italy
^jUniversità di Firenze, Firenze, Italy
^kUniversità di Genova, Genova, Italy
^lUniversità degli Studi di Milano, Milano, Italy
^mUniversità di Milano Bicocca, Milano, Italy
ⁿUniversità di Modena e Reggio Emilia, Modena, Italy
^oUniversità di Padova, Padova, Italy
^pUniversità di Perugia, Perugia, Italy
^qScuola Normale Superiore, Pisa, Italy
^rUniversità di Pisa, Pisa, Italy
^sUniversità della Basilicata, Potenza, Italy
^tUniversità di Roma Tor Vergata, Roma, Italy
^uUniversità di Siena, Siena, Italy
^vUniversità di Urbino, Urbino, Italy
- [†]Deceased